Stannides and Intermetallic Tin Compounds – Fundamentals and Applications

Rainer Pöttgen

Institut für Anorganische und Analytische Chemie, Westfälische Wilhelms-Universität Münster, Corrensstraße 30, D-48149 Münster, Germany

Reprint requests to R. Pöttgen. E-mail: pottgen@uni-muenster.de

Z. Naturforsch. **61b,** 677 – 698 (2006); received January 19, 2006

Dedicated to Professor Wolfgang Jeitschko on the occasion of his 70th birthday

Tin, tin alloys and intermetallic tin compounds play a key role in many technologies and high-tech applications. Many of these intermetallics find application in daily life such as pewterware, bronzes, solders, fusible alloys, superconductors, capsules for wine bottles or tinplate packaging. Many of the applications are directly related to distinct stannides or intermetallic tin compounds. The crystal chemistry and chemical bonding of these materials as well as their applications are briefly reviewed.

Key words: Tin, Stannides, Intermetallics

Introduction

Elemental tin is a fascinating element which has two modifications under ambient pressure conditions. At 13.2 °C the tetragonal metallic β-modification (space group $I4_1/amd$, $\rho = 7.285$ g/cm^3) transforms to the semi-metallic α-modification with the cubic diamond structure (space group $Fd\bar{3}m$, $\rho = 5.769$ g/cm^3) [1, 2]. This phase transition proceeds *via* a *translationengleiche* symmetry reduction [3] and usually proceeds slowly. However, if small nuclei of the α-modification have formed, the transformation proceeds rather fast and destroys the metallic workpiece (tin pest). The two modifications have different near-neighbor coordination. In α-Sn each tin atom has a tetrahedral coordination at a Sn–Sn distance of 281 pm, while the coordination number in β-Sn is increased to $4 \times 302 + 2 \times 318$ pm (Fig. 1).

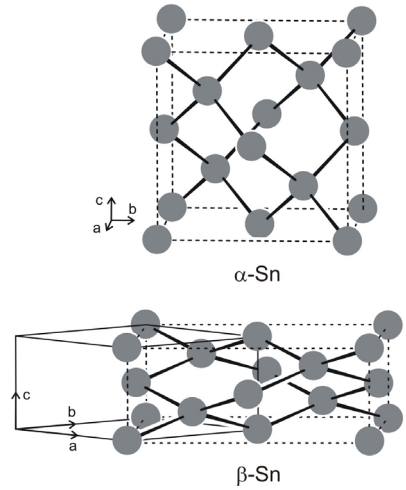

Fig. 1. The structures of α- and β-Sn. The tetragonal unit cell of β-Sn is drawn with a solid line. The compressed cubic cell is drawn with dotted lines for comparison.

Tin is a relatively soft metal with a good ductility. This is the prerequisite for the use as tinfoil (silverpaper), *e. g.* for capsules for wine bottles. When bending small tin bars (Fig. 2), one notices a peculiar sound which is known as the tin cry. The latter results from the friction of small crystallites in the β-modification. A sound reception of the tin cry can be obtained from the internet [4]. The bending of a tin bar leaves small fractures at the surface.

Tin is a metal typically used in daily life for various tin vessels, as pewterware or for different objects of art. For many technical applications tin is alloyed with other metals. Typical alloy systems are the various Cu–Sn bronzes, britannia metal (a Sn-Sb-Cu alloy) or bronzes alloyed with P, Zn, Pb, Si, in order to enhance the hardness and mechanical workability, or to improve the electrical properties. In most cases, multinary compounds / alloys are used for technical application. All these aspects are competently reviewed in the Tin Handbook [5].

Fig. 2. A molten and a bent tin bar. For details see text.

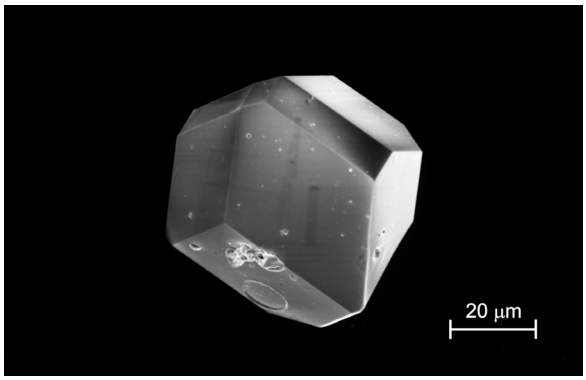

Fig. 3. A single crystal of Ir_3Sn_7 grown from liquid tin.

Herein we present new aspects and focus on intermetallic compounds formed by tin and alkali, alkaline earth, transition, rare earth, and actinoid metals. This review is written from the preparative solid state chemist's point of view. In the following chapters, we can mention characteristic stannides only in passing, and we focus on typical aspects of stannide chemistry. Complete crystallographic data of the plethora of known compounds can be found in many compilations [6, 7] and in the modern electronic data bases [8].

Syntheses Conditions

Tin melts at 232 °C and has an enormous liquidus range with a high boiling temperature of 2687 °C [9]. Furthermore, tin has an excellent wettability for many metals and this is a big advantage for the synthesis. The high boiling point is favourable for synthesis, since one does not risk tin evaporation. The simplest method for the preparation of metal stannides is the melting of the elements in sealed, evacuated silica tubes or in ceramic (Al_2O_3 or ZrO_2) crucibles in a vacuum or under inert gas atmosphere. Also glassy carbon is a suitable, inert container material.

In order to avoid the contact with a container or crucible material, arc-melting [10] of the elements on a water-cooled copper chill or within a conical crucible is a widely used technique for the preparation of stannides. An advantage of the arc-melting procedure is the possibility to generate very high temperatures in a short time. Since the contact area of the molten sample with the water-cooled copper chill is very small, this technique is often called quasi-crucible-free melting. Similar results can be obtained *via* induction [11, 12] or induction levitation melting of the elements. In some cases, annealing of the samples in a high-frequency furnace improves the crystal quality.

While tin has this large liquidus range, some metals, *i. e.* alkali and alkaline earth metals, europium, ytterbium, and manganese have comparatively low boiling temperatures and high vapour-pressures [9]. Binary and ternary stannides of these elements can only be prepared in sealed high-melting metal tubes (niobium or tantalum). These reaction containers are subsequently sealed in evacuated silica ampoules for oxidation protection. Details about the handling of these inert crucible materials have been summarized by Corbett [13].

The low melting point and the excellent wettability are good prerequisites for the tin flux technique. Besides the self-flux technique for the growth of tin-rich stannides, liquid tin can widely be used for the growth of other crystals. Jolibois already used liquid tin for the growth of NiP_3 crystals [14]. Silica tubes, ceramic (Al_2O_3 or ZrO_2), niobium or tantalum crucibles are suitable container materials for the tin flux reactions. The excess tin can easily be dissolved in hydrochloric acid, provided that the binary or ternary compound is stable under these conditions. A detailed overview on the tin flux technique is given in a recent review article devoted to the many metal flux possibilities [15]. As an example for crystals grown from a tin flux we present well-shaped crystals of Ir_3Sn_7 [16] in Fig. 3.

Stannides can also be produced as nanoparticles. An interesting approach is the polyol route that has recently been used for the synthesis of the stannides $AuNiSn_2$ and $AuCuSn_2$ [17]. In a typical reaction tetrachlorogold acic $HAuCl_4 \cdot 3H_2O$, copper acetate, $SnCl_2$, and polyvinylpyrrolidone in tetraethylene glycol are reduced at 70 °C with a solution of $NaBH_4$, fol-

lowed by heating to 120 – 200 °C for 10 min. The correct structures of these stannides, however, have later been determined from crystals grown under conventional synthesis conditions [18].

In the large field of catalysis, stannides are often required as thin films on ceramic supports. Such films can either be generated through evaporation of tin on a noble metal surface under ultrahigh vacuum conditions [19] or *via* thermolysis of metal-organic coordination polymers [20].

Stannides of the Alkali and Alkaline Earth Metals

Most phase diagrams of the binary systems of the alkali and alkaline earth metals with tin are compiled in the Massalski Handbook [6]. Although many of the binary phase diagrams have been investigated already a century ago, the information to be gained from these phase diagrams, however, is limited, and many phases are still unknown. The number of new binary alkali and alkaline earth metal stannides reported in recent years [21 – 34] is remarkable.

The Li–Sn phases [28, 35 – 41] have intensively been investigated with respect to their use for battery materials [42, 43]. The use of binary lithium stannides instead of elemental lithium foil strongly reduces the formation of whiskers during the reduction process. It is worthwhile to note that the structure of $Li_{4.4}Sn$ has only recently been studied on the basis of neutron diffraction data [28]. The binary lithium stannides have also been characterized in detail through their ^{119}Sn Mössbauer data, thermodynamic behaviour, and electronic structure calculations [44 – 48]. A common structural motif of the different structures of the lithium stannides are distorted, tungsten related cubes of lithium and tin atoms around each lithium atom [39].

The crystal chemistry and chemical bonding in the alkali metal–tin systems have recently competently been reviewed by Fässler and Hoffmann [49]. Several new phases, especially of sodium have been reported in recent years. These stannides exhibit an enourmous structural variety. To give some examples: 2D realgar-type units $[Sn_8]^{4-}$ in $NaSn_2$ [32], nineteen crystallographically independent tin sites in the 3D polyanion ($[Sn^0]_{128}[Sn^-]_{80}$) of Na_5Sn_{13} [22], or a 3D network with two-, three-, and four-bonded tin atoms in Na_7Sn_{12} [29]. Most recently the vacancy ordering in the type-I tin clathrate $Rb_8Sn_{44}\square_2$ [34] was established on the basis of precise single crystal X-ray data. Also the defect clathrate Cs_8Sn_{44} has been reported [50]. These clathrate phases are promising candidates for thermoelectric materials [51 – 53]. The systems with potassium, rubidium, and cesium have not so intensively been investigated as the sodium–tin system. Some of the structures have still not been solved [6, 49]. Structure refinements have been reported for the tetrastannides A_4Sn_4 (A = Na, K, Cs) [54, 55] and for a variety of structurally complex stannides like K_4Sn_9 [57, 58] or $Cs_{52}Sn_{82}$ [59] which contain the Sn_9^{4-} cluster anion (Fig. 4).

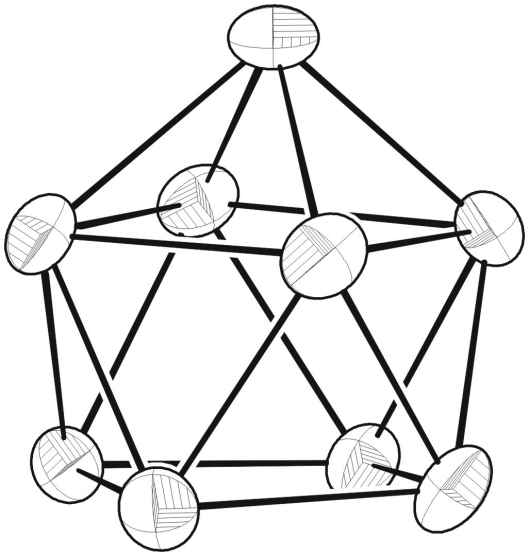

Fig. 4. The Sn_9^{4-} cluster anion in K_4Sn_9 [56].

Many of the alkali and alkaline earth metal stannides show tin substructures that can easily be understood with the Zintl-Klemm concept. An overview on the many compounds is given in two review articles [49, 60]. Two prominent examples are Mg_2Sn [61] and SrSn [62]. Mg_2Sn occurs as a precipitation in modern light weight magnesium alloys and is also discussed as an electrode material for battery applications. Considering the charge transfer from the two magnesium atoms to the tin atoms, we obtain an isolated Sn^{4-} Zintl anion with [Xe] electron configuration. These Sn^{4-} anions build up a cubic close packed arrangement in which all tetrahedral sites are filled with magnesium (Fig. 5). This corresponds to an anti-fluorite type arrangement.

For SrSn we obtain an ionic formula splitting $Sr^{2+}Sn^{2-}$, and the tin anions have the valence electron concentration of tellurium and consequently the tin atoms form two covalent bonds leading to zig-zag

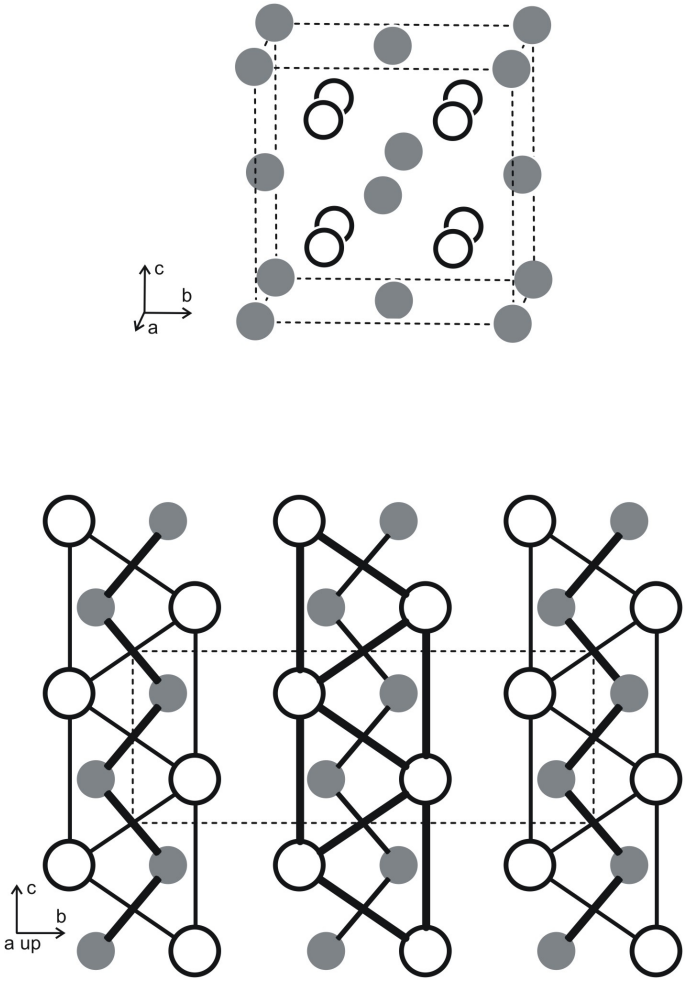

Fig. 5. The crystal structures of Mg_2Sn (upper drawing) and SrSn. The alkaline earth metal and tin atoms are drawn as open and medium grey circles, respectively. The trigonal prismatic units around the tin atoms in SrSn are shifted by half the translation period *a*, indicated by thin and thick lines.

chains (Fig. 5) at what is almost a Sn–Sn single bond distance of 294 pm. Each tin atom obtains a trigonal-prismatic strontium coordination. Layers of condensed prisms are shifted by half a translation period. Several other of these stannide Zintl phases are dicussed in [63].

Besides these two simple examples, also some more complex phases have been observed in the alkaline earth metal–tin systems [49]. Ca_2Sn, Sr_2Sn, Ba_2Sn, and the mixed stannides CaMgSn, SrMgSn, and BaCaSn crystallize with an *anti*-$PbCl_2$ type structure with isolated Sn^{4-} anions. $BaSn_3$ [27], $SrSn_3$ [25], and $SrSn_4$ [30] are superconductors with transition temperatures of 2.4, 5.4, and 4.8 K, respectively. Chemical bonding in the tin substructures of these stannides has intensively been investigated on the basis of LMTO band structure calculations and the electron localization function. The calculations reveal lone pairs at the tin sites and the role of these lone pairs is discussed with respect to the superconducting properties [27].

Divalent ytterbium and europium have ionic radii similar to calcium and strontium [9]. Consequently one observes compounds of similar composition and with similar bonding patterns. To give an example, EuSn and YbSn both crystallize with the orthorhombic CrB type structure, similar to SrSn discussed above. The phase diagrams Eu–Sn [64] and Yb–Sn [65] have recently been updated.

An interesting approach is the synthesis of mixed alkali–alkaline earth–metal stannides, since the use of two cations of different size enables the stabilization of different tin substructures. The stannide $Sr_{2.04}Ca_{0.96}Sn_5$ [33] can be considered as a solid solution of calcium in the stannide Sr_3Sn_5. The tin sub-

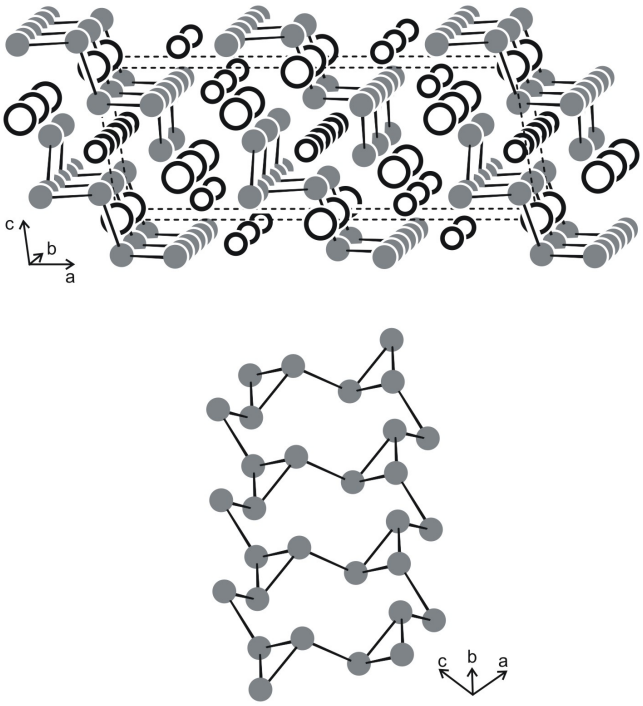

Fig. 6. The crystal structure of $Ba_3Li_4Sn_8$. The barium, lithium, and tin atoms are drawn as large open, small open, and medium grey circles, respectively. The one-dimensionally infinite tin polyanion is emphasized and a cutout is presented in the lower part.

structure consists of isolated, slightly distorted square-pyramidal Sn_5^{6-} units. At low temperature (100 K) $Sr_{2.04}Ca_{0.96}Sn_5$ shows a bond-stretching isomerism, *i. e.* the square pyramids contract and the intra-cluster Sn–Sn bonds shorten, while the inter-cluster bonds become very large.

A peculiar tin substructure occurs in $Ba_3Li_4Sn_8$ [66]. As emphasized in Fig. 6, a one-dimensional tin substructure is embedded in a matrix of barium and lithium atoms. The $^1_\infty[Sn_8]^{10-}$ chains consist of three- and ten-membered rings at Sn–Sn distances ranging from 288 to 311 pm. The monomeric ten-membered ring has the shape of cyclodecane in an all-chair conformation. Considering the two-bonded Sn^{2-} and three-bonded Sn^{1-} tin anions, the compound can be described as an electron precise Zintl phase $(Ba^{2+})_3(Li^+)_4[(Sn^{2-})_2(Sn^-)_6]$.

Other recent examples for mixed cation stannides are $CaNa_{10}Sn_{12}$ and $SrNa_{10}Sn_{12}$ [67]. These compounds contain the large isolated cluster $[Sn_{12}]^{12-}$ which has the shape of a giant truncated tetrahedron. These clusters are arranged in a cubic body centered way. All tin atoms are three-bonded Sn^- species. Ternary stannides with smaller and larger cations have more systematically been investigated in recent years by the Sevov group [68 – 71]. The stannides $A_3Na_{10}Sn_{23}$ (A = K, Rb, Cs) [69] contain fused pentagonal dodecahedra and layers of isolated tin tetrahedra. An *arachno*-$[Sn_8]^{6-}$ cluster occurs in $A_4Li_2Sn_8$ (A = K, Rb) [71].

Really spectacular are the stannides Na_8BaSn_6, Na_8EuSn_6 [68], $Li_5Ca_7Sn_{11}$, and $Li_6Eu_5Sn_9$ [70]. The two sodium based stannides contain cyclopentadienyl anion analogues Sn_5^{6-}, while similar five-membered rings besides Sn_6 chains are realized in $Li_5Ca_7Sn_{11}$. In $Li_6Eu_5Sn_9$ the Sn_5 rings are separated by infinite zig-zag chains. Na_8EuSn_6 orders magnetically around 20 K [68]. The signal observed near 70 K most likely resulted from a minor impurity of ferromagnetic EuO [72, 73]. The stannide CaLiSn [74] adopts a superstructure of the AlB_2 type with an ordering of the lithium and tin atoms on the boron network. The three different [LiSn] networks are all slightly puckered.

Some stannide formulae are not electron precise and cannot be formulated with an ionic formula splitting. Such an example is *Sr*$_3$*Sn* which is indeed Sr_3SnO with an *anti*-perovskite structure with oxygen atoms in the strontium octahedra [62]. The compound can then be formulated as $(Sr^{2+})_3Sn^{4-}O^{2-}$. A similar phase, Eu_3SnO has been observed with divalent europium [75, 76]. Even more interesting is the

structure of $Cs_{48}Sn_{20}O_{21}$ [77]. This stannide stannate can be understood proposing an ionic formula $Cs_{48}[Sn_4]_4[SnO_3]_4[O]_7[O_2]$ containing the Zintl anions Sn_4^{4-} with three-bonded tin atoms.

A particularly pervasive problem are hydrogen impurities. The source of the hydrogen is mostly the commercially available alkaline earth metal. The main problem is always the detection of hydrogen in heavy atom compounds by common X-ray diffraction techniques. In those cases, where a hydrogen contamination is assumed, neutron diffraction on deuterated samples is an adequate technique. The hydrogen containing samples can also be burned in an oxygen atmosphere and the resulting water can be titrated potentiometrically by the Karl-Fischer technique [78]. Hydrogen stabilization was observed for a variety of stannides, *e. g.* $Ca_5Sn_3H_x$, $Ba_5Sn_3H_x$, $Eu_5Sn_3H_x$, or Ca_3SnH_x [79 – 81].

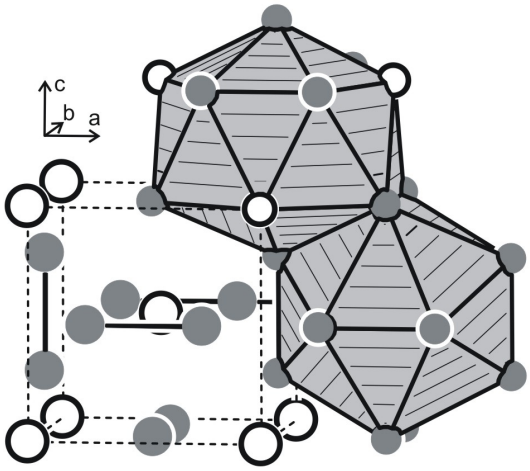

Fig. 7. The crystal structure of Nb_3Sn. The niobium and tin atoms are drawn as medium grey and open circles, respectively. The CN 14 and CN 12 (right-hand part) polyhedra around the niobium and tin atoms are emphasized.

Transition Metal Stannides

Binary stannides

First reports on some binary transition metal (T)–tin systems have already been published one hundred years ago [7]. Many crystallographic data and parts of the phase diagrams can be found in the Pearson [7] and Massalski [6] Handbooks. Similar to the alkali and alkaline earth metal based systems discussed above, also several T_xSn_y structures have structurally been studied only recently. The enthalpies of formation have been studied for several binary stannides [82].

The structural chemistry of the T_xSn_y stannides differs significantly from that of the alkali and alkaline earth metal based systems. The T_xSn_y compounds should be considered as intermetallic compounds. Most of them show metallic conductivity and Pauli paramagnetism. Several structures show strong *T*–Sn bonding.

The structure of Ti_2Sn_3 was determined recently by two independent groups [83, 84]. Ti_2Sn_3 can directly be synthesized from the elements and single crystals can be obtained *via* chemical transport using iodine as the transport agent. Metallic behaviour was evident from electronic structure calculations and experimentally manifested by susceptibility and resistivity measurements. In the Ti_2Sn_3 structure one observes a complex interplay of Ti–Ti, Ti–Sn, and Sn–Sn interactions. The structures of Zr_5Sn_3 (Mn_5Si_3 type) and Zr_5Sn_4 (filled Mn_5Si_3 type) have recently been refined [85]. These investigations were carried out in a broader context in order to study the filling of octahedral voids in the Mn_5Si_3 (Nowotny) phases.

The stannides VSn_2, $NbSn_2$, and $CrSn_2$ [86] have been fully characterized on the basis of single crystal data. Quantitative synthesis is possible *via* the tin flux technique. The tentative compositions V_2Sn_3 and Cr_2Sn_3 previously assigned in the literature have been corrected. These three stannides crystallize with the orthorhombic Mg_2Cu type structure. Resistivity measurements reveal metallic behaviour for $CrSn_2$ and $MoSn_2$ [87]. The latter stannide crystallizes with the hexagonal Mg_2Ni structure. Both structure types are closely related. The electronic structures of the stannides with Mg_2Ni and Mg_2Cu type structures have been studied in detail and the role of the valence electron concentration has been discussed [88].

A technically important group V transition metal stannide is Nb_3Sn with the β-tungsten structure (Fig. 7). Both atom types have Frank-Kasper [89, 90] polyhedra: CN 12 for Sn (niobium icosahedron) and CN 14 for Nb (10 Nb + 4 Sn). These polyhedra are condensed *via* common triangular faces. Metallic Nb_3Sn has a certain ductility and it is a commonly used superconducting material with a transition temperature of 18 K [91].

Some stannides form complex superstructures of simple subcell variants. The superstructure formation can be due to occupation modulation. Recent examples for such phases with superstructures that derive from

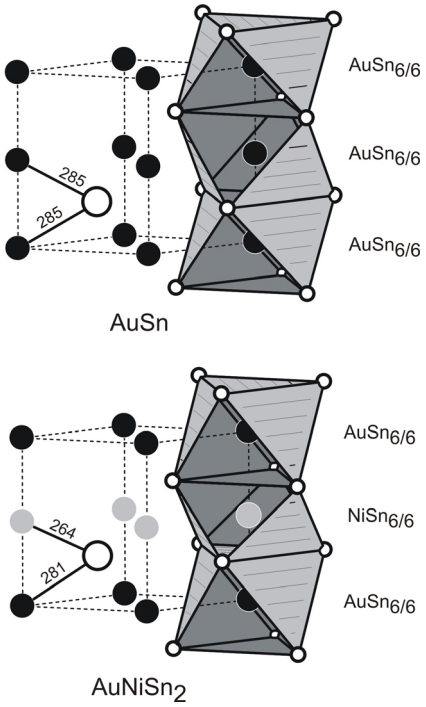

Fig. 8. The crystal structures of AuSn and $AuNiSn_2$. Gold, nickel, and tin atoms are drawn as black, light grey, and open circles, respectively. The different chains of face-sharing octahedra are emphasized.

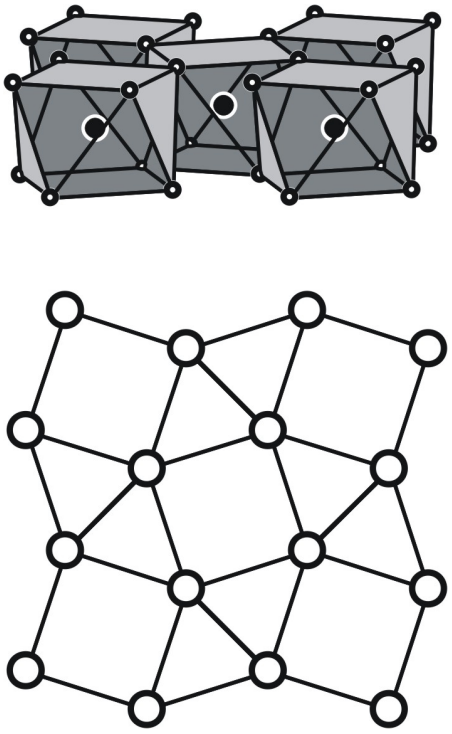

Fig. 9. A layer of edge-sharing $PdSn_{8/2}$ square antiprisms (upper drawing) and the $3^2.4.3.4$ network in the structure of $PdSn_4$. For details see text.

the NiAs/Ni_2In structural family are Mn_8Sn_5 [92], HT–$Ni_{1+\delta}Sn$ ($\delta = 0.28, 0.52, 0.61$) [93], LT–$Ni_{1+\delta}Sn$ ($\delta = 0.47,\ 0.50$), and LT'–$Ni_{1+\delta}Sn$ ($\delta = 0.35,\ 0.38,\ 0.41$) [94]. The structure of Ni_3Sn has been reinvestigated on the basis of single crystal data in order to get good starting values for electronic structure calculations [95]. The Ni–Sn interactions were found to be stronger than the Ni–Ni interactions in the octahedral Ni_6 cluster chains.

The stannide AuSn adopts the NiAs type (Fig. 8). The gold atoms build up linear chains along the *c* axis with Au–Au distances of 276 pm. All gold atoms have an octahedral tin coordination. The recently synthesized stannides $AuNiSn_2$ and $AuCuSn_2$ [17, 18] adopt an ordered version of AuSn, where every other gold atom is replaced by nickel and copper, respectively. Due to the difference in size between gold and nickel (copper) one observes smaller and larger octahedra in the ternary stannides leading to a symmetry reduction.

A new stannide Os_4Sn_{17} was synthesized from the elements *via* the tin flux method and the complex orthorhombic structure was determined from single crystal data [96]. The structure contains two crystallographically independent osmium sites. It is interesting to note that the Os2 atoms have nine tin neighbours. Single crystals of Os_3Sn_7, $RhSn_3$, $RhSn_4$, $IrSn_4$, Ir_5Sn_7, $Ni_{0.402}Pd_{0.598}Sn_4$, α-$PdSn_2$, and $PtSn_4$ have also been grown from liquid tin and the structures were precisely refined from diffractometer data [97]. Many of these compounds had been already known, but the structural information was based either on powder or single crystal film data.

Another family of binary transition metal stannides (*e. g.* $PdSn_2$ [98], α- and β-$CoSn_3$ [99], $PtSn_4$, β-$IrSn_4$, $PdSn_3$, $PdSn_4$ [100]) has common structural characteristics, *i. e.* a square antiprismatic coordination of the transition metal atoms and a stacking of $3^2.4.3.4$ nets (Fig. 9). The only difference between these structures is the stacking sequence of the layers of condensed square antiprisms. In some cases, the layers are directly condensed *via* the square faces leading to double prisms, and consequently one observes *T*–*T* dumbbells. In Fig. 10 we present the structure of β-$CoSn_3$ as an example. The different packing schemes of the other structures are summarized in [100]. An interesting situation occurs for the stannide $PdSn_3$ (Fig. 11) which

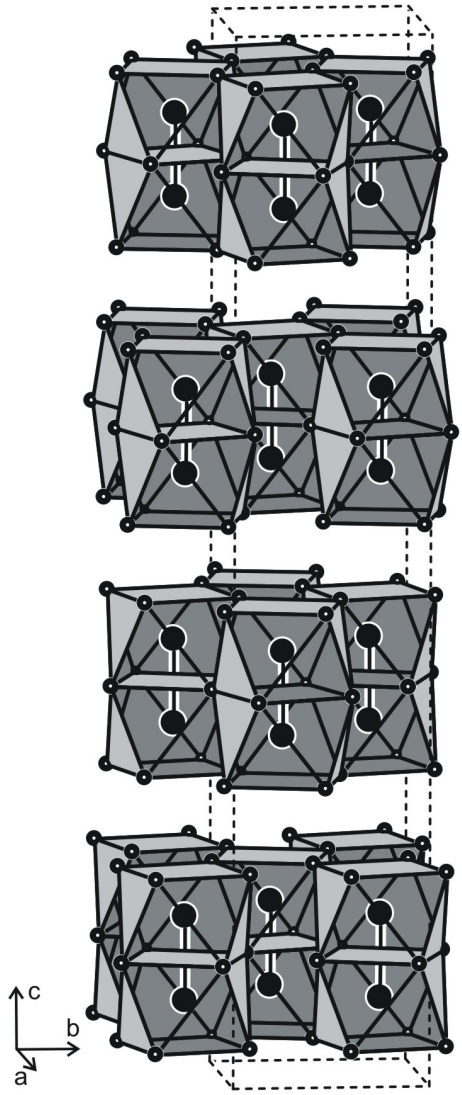

Fig. 10. The crystal structure of β-$CoSn_3$. The square antiprisms around the Co_2 dumb-bells are emphasized. For details see text.

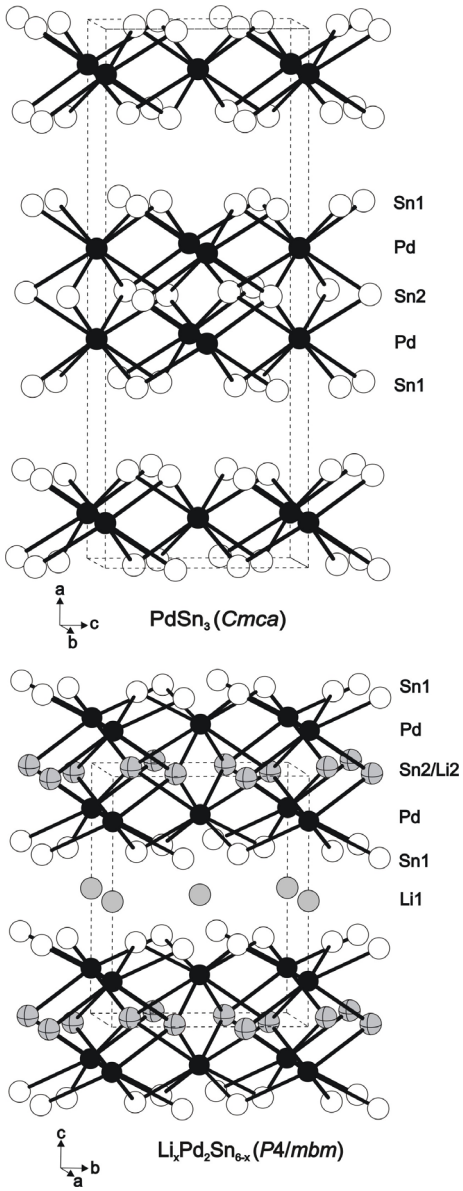

Fig. 11. The crystal structures of $PdSn_3$ and $Li_{1+x}Pd_2Sn_{6-x}$. The two-dimensional $[Pd_2Sn_6]$ networks are emphasized. For details see text.

has square antiprismatic voids between the $PdSn_3$ layers. This compound can be intercalated with lithium, leading to the stannides $Li_{1+x}Pd_2Sn_{6-x}$ ($x = 0.40-0.46$) [101]. However, there is a significant difference between the structures of $PdSn_3$ and $Li_{1.42}Pd_2Sn_{5.58}$ (Fig. 11). The lithium atoms intercalating between the $PdSn_3$ layers need a square prismatic coordination, and consequently, every other $PdSn_3$ layer needs to rotate by about 45°. Furthermore, the tin position within the $PdSn_3$ layer shows Sn/Li mixing. As is evident from electronic structure calculations, this Sn/Li substitution reduces the total electron count and induces the formation of this peculiar structure.

Solders, precipitations and tinning

Binary transition metal stannides also occur at the interface between solders and contacts of electronic devices [102–104]. Technically important binaries are the palladium stannides, Ni_3Sn_4, $(Cu, Ni)_3Sn_4$,

Cu_6Sn_5, (Cu, Ni)$_6Sn_5$, Cu_3Sn, Ag_3Sn, Ag_3(Sn, Sb), AuSn, $AuSn_2$, $AuSn_4$, FeSn, $FeSn_2$, and Ni_3Sn_2 [5, 105, 106]. A current research interest is the search for lead-free solders for high-tech electronics, since the European Union has decided to ban the use of lead-based solders soon.

The binary iron stannides form during each tinning process of iron based plates. They are responsible for the binding of the tin coating to the plate. In former time cans have been coated with tin for corrosion protection. Nowadays most cans are coated with polymers.

Catalyses and battery materials

Transition metal stannides are important catalytically active materials for different applications, mostly in heterogeneous catalysis [19, 20, 107 – 113]. In commercial calatysts for reforming applications, platinum is always used in combination with a second element. In that context, the platinum stannides Pt_3Sn and Pt_2Sn have been discussed as surface alloys [114]. These stannides have also been studied as model systems for the cyclohexane conversion to benzene [19]. Modified platinum catalysts have intensively been investigated for the naphtha reforming process (production of high-octane gasoline) [115 – 118]. For the latter process, however, in most cases mixed oxidic/metallic catalysts have been tested. The stannide phases formed *via* reduction in hydrogen flow. Co/Sn and Ru/Sn calatysts are used for the large scale production (more than one million tons per year) of fatty alcohols [119].

The binary intermetallic Cu–Sn alloys are technologically important for the various applications of art-bronzes and other materials. All these alloys are used in amounts of tons in daily life. Another very important topic concerns the use of tin-based intermetallic compounds and alloys for new anode materials for lithium ion batteries [120 – 128, and ref. therein], since such materials exhibit high specific capacities. An overview on the currently investigated stannides, *i. e.* Cu_6Sn_5, $MnSn_2$, $Mn_{1.77}Sn$, Mn_3Sn, FeSn, $FeSn_2$, $CoSn_2$, Ag_3Sn, and Ni_3Sn_2, is given in [123]. Among these stannides especially Cu_6Sn_5 has widely been studied [126 – 128]. Electrochemical studies gave hints to a product $Li_xCu_6Sn_5$ ($x \approx 13$) [126], however, from a crystal chemical point of view, this is questionable, since the lithium incorporation would significantly increase the valence electron concentration. Detailed preparative solid state work is needed on all these materials to get proofs on the structures and compositions of these compounds. Also a combination of *in situ* X-ray diffraction and electrochemistry can help to solve these problems.

Ternary transition metal stannides and thermoelectrics

Ternary systems *T*–*T'*–Sn have also been investigated in order to study solid solutions and to find new ternary stannides. Nickel coated with a thin gold layer is commonly used as a metallization in electronics packaging. The reaction of this layer with tin based solders can result in the formation of transition metal stannides. The system Au–Ni–Sn has been studied in detail with respect to such materials [129, 130]. Nickel atoms can substitute gold in $AuSn_4$ leading to a solid solution $Au_{1-x}Ni_xSn_4$ ($x \leq 0.5$). All these stannides crystallize with the $PdSn_4$ structure with a square antiprismatic coordination of the transition metal atoms.

The manganese based stannides are interesting magnetic materials. $TiMnSn_4$ adopts an ordered version of the hexagonal Mg_2Ni type [131]. This metallic stannide shows temperature dependent paramagnetism in the temperature range 100 to 300 K. Similar to the Au–Ni–Sn system, also the Au–Mn–Sn system [132 – 134] is technologically interesting with respect to electronic circuits [135]. The knowledge of the phase diagrams is essential to the engineering of materials. The MgAgAs type structure of MnAuSn was clearly established from X-ray single crystal and neutron powder diffraction data. There is no evidence for Mn/Sn disorder in the MnAuSn structure. This stannide orders ferromagnetically around 600 K with a magnetic moment of 3.62 μ_B/Mn atom in the ordered state.

The stannides ZrNiSn and $ZrNi_2Sn$ have already been reported in 1970 by Jeitschko [136]. Equiatomic ZrNiSn adopts the half-Heusler structure (MgAgAs type) and $ZrNi_2Sn$ crystallizes with the Heusler type structure. Although $ZrNi_2Sn$ may be described as a filled-up variant of ZrNiSn, these two stannides do not form a continuous solid solution. The stannide ZrNiSn and related materials have recently been intensively been reinvestigated with respect to their thermoelectric properties [137 – 140, and ref. therein]. For ZrNiSn already 59 entries occur in the SciFinder data base [8]. Uher and coworkers could show that the transport in ZrNiSn is extremely sensitive to the structural arrangements and can effectively be manipulated by alloying and doping.

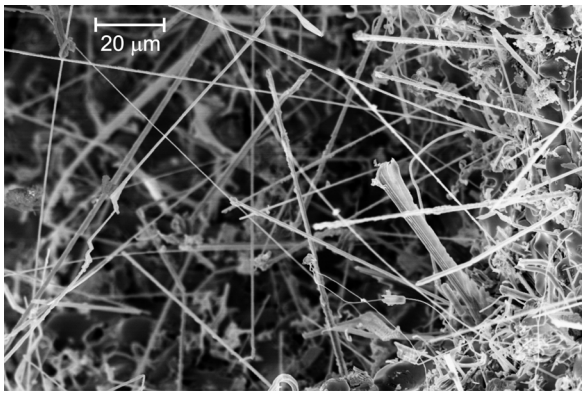

Fig. 12. Scanning electron micrograph of the corroded surface of a YbPtSn sample.

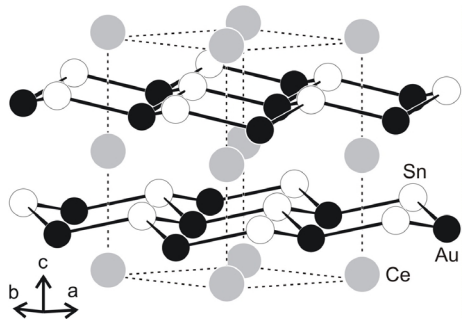

Fig. 13. The crystal structure of CeAuSn. Cerium, gold, and tin atoms are drawn as light grey, black, and open circles, respectively. The two-dimensional [AuSn] network is emphasized.

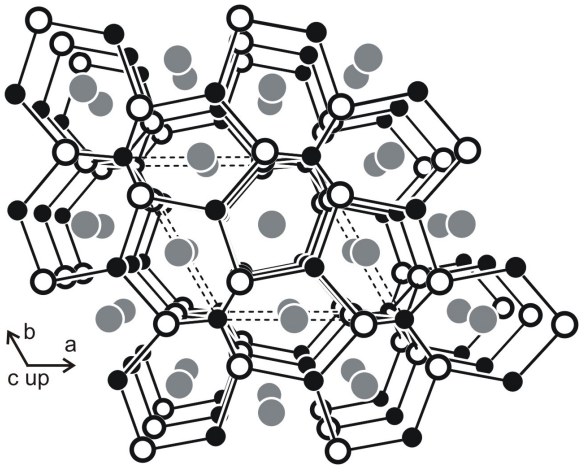

Fig. 14. Perspective view of the CeRhSn structure along the *c* axis. Cerium, rhodium, and tin atoms are drawn as medium grey, black, and open circles, respectively. The three-dimensional [RhSn] network is emphasized.

Stannide oxides – corrosion products

The purity of educts and samples is always an important question concerning the stability of compounds and furthermore the physical properties, *e. g.* magnetic and electrical data. Titanium, zirconium, and hafnium are frequently used as reactive getters due to their affinity to oxygen. This is a severe problem for the synthesis of intermetallic compounds, since the latter may also act as oxygen traps. In the field of stannides the influence of oxygen on the stability of Zr_4Sn was studied by Kwon and Corbett [141].

A yet not understood oxidation/hydrolysis process occurs for tin-rich binary and ternary compounds. Samples of $MnSn_2$ show whisker growth after exposure to air. Already after one day whiskers with a length up to 500 μm occur [142]. Similar whiskers have also been observed during a long-term exposure of the ternary stannides $CaTSn_2$ (T = Rh, Pd, Ir), YbPtSn and various indides [143]. As an example we present a scanning electron micrograph of a corroded YbPtSn sample (Fig. 12). Some of the whiskers have lengths around 200 μm.

During the reaction of titanium with rutile and tin at 1500 °C Hillbrecht and Ade obtained the new compound $Ti_{12}Sn_3O_{10}$ [144], a low-valent oxide with an oxidic network and intermetallic *islands*. Within the intermetallic part, one observes a substantial degree of Ti–Ti and Ti–Sn bonding, while the oxygen atoms within the oxidic network build up OTi_4 tetrahedra and OTi_5 bipyramides.

Similar oxidation products have been obtained with the late transition metals. The structures of $Ru_3Sn_{15}O_{14}$ [145], $Os_3Sn_{15}O_{14}$ [146], and $Fe_4Si_2Sn_7O_{16}$ [147] contain $RuSn_6$, $OsSn_6$, and $FeSn_6$ octahedra. $Ir_3Sn_8O_4$ [148] is a cluster compound with an incommensurably modulated structure with $IrSn_6$ octahedra.

Ternary Stannides with [T_xSn_y] Polyanions

Rare earth metal based stannides

The crystallographic data and basic physical properties of the binary rare earth metal stannides are summarized in a recent review by Skolozdra [149]. Many of the RE_xSn_y stannides crystallize with structures that are typical for the binary transition metal stannides, but some stannides adopt their own structure types. So far not all structures of the RE_xSn_y stannides are known and some of the phase diagrams are still incomplete. As discussed above, the phase dia-

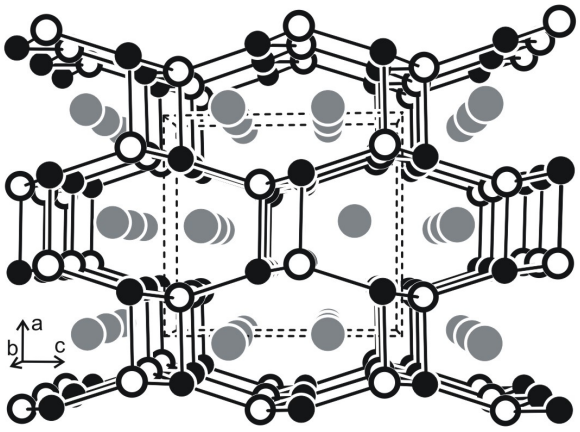

Fig. 15. Perspective view of the NP-CePtSn structure along the *b* axis. Cerium, platinum, and tin atoms are drawn as medium grey, black, and open circles, respectively. The three-dimensional [PtSn] network is emphasized.

grams Eu–Sn [64] and Yb–Sn [65] have been updated recently.

A really fascinating family of intermetallic tin compounds are the rare earth (*RE*)–transition metal (*T*)–stannides of general composition $RE_xT_ySn_z$. These intermetallics have intensively been investigated in the last thirty years and the wealth of data has been summarized in a recent review article by Skolozdra [149]. The $RE_xT_ySn_z$ stannides are a very large family of compounds with greatly differing crystal structures and manifold physical properties. So far more than 400 compounds have been synthesized. For crystallographic details we refer to the review article, and only some representative compounds are discussed herein.

Many of the $RE_xT_ySn_z$ stannides (T = late transition metal) have a common pattern of chemical bonding. The rare earth metal atoms as the most electropositive component largely transfer their valence electrons to the transition metal and tin atoms, thus enabling covalent bonding between these elements. As a consequence one obtains two- or three-dimensional $[T_ySn_z]$ polyanionic networks that are charge balanced and separated by the rare earth cations. Although all these materials are metals, semi-metals or semiconductors, one observes a significant degree of covalent *T*–Sn bonding [150, 151]. As representative examples the structures of CeAuSn [152], CeRhSn, the normal-pressure modification of CePtSn, and $Sm_2Cu_4Sn_5$ [153] are presented in Figs 13 – 16. While CeAuSn shows a pronounced two-dimensional [AuSn] network with fully ordered Au_3Sn_3 hexagons, the networks in CeRhSn

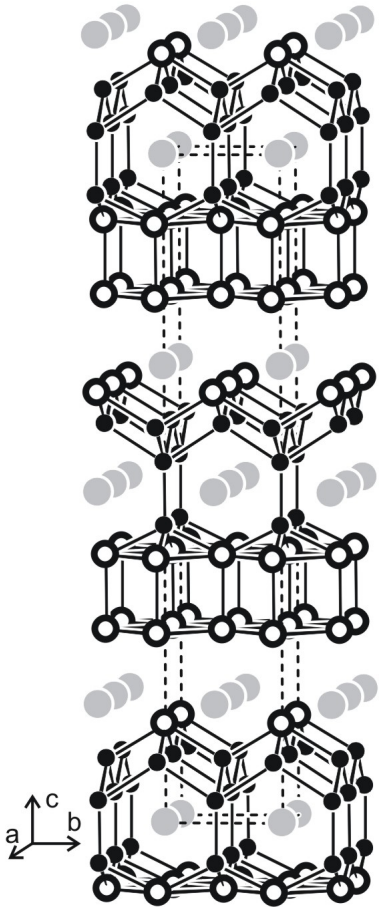

Fig. 16. The crystal structure of $Sm_2Cu_4Sn_5$. The samarium, copper, and tin atoms are drawn as light grey, black, and open circles, respectively. The two-dimensional $[Cu_4Sn_5]$ network is emphasized.

(ZrNiAl type) and NP-CePtSn (TiNiSi type) are three-dimensional. $Sm_2Cu_4Sn_5$ (own type) shows complex two-dimensional $[Cu_4Sn_5]$ networks which are connected *via* the samarium atoms. The shortest Sn–Sn contacts between these networks at 415 pm are certainly not bonding. Most other $RE_xT_ySn_z$ stannides show similar crystal chemistry and bonding patterns.

The equiatomic *RET*Sn stannides have intensively been investigated with respect to their magnetic properties. Most of these compounds crystallize with the ZrNiAl type or they adopt ordered superstructures of the AlB_2 type. A detailed overview on the physical properties of the *RET*Sn stannides is given in the *Handbook of Crystal Structures and Magnetic Properties of Rare Earth Intermetallics* by Szytuła and Leciejewicz [154]. Especially the cerium com-

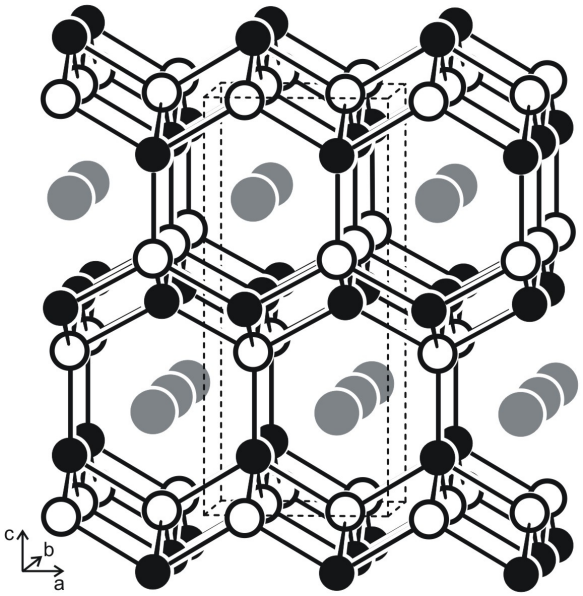

Fig. 17. The crystal structure of $CePt_2Sn_2$. Cerium, platinum, and tin atoms are drawn as medium grey, black, and open circles, respectively. The three-dimensional $[Pt_2Sn_2]$ network is emphasized.

pounds [155] have been studied extensively since they can exhibit valence changes or valence instabilities, *i. e.* [Xe]$4f^0$ vs [Xe]$4f^1$. For the valence fluctuating Kondo lattice system CeNiSn already 208 entries can be found in the SciFinder data base [8]. Also the intermediate valence system CeRhSn [151, 156, and ref. therein] with strongly correlated electron behaviour and the normal pressure modification NP-CePtSn [150, and ref. therein] have thouroughly been studied.

Some of the Ce*T*Sn stannides show phase transitions under high-pressure conditions. NP-CePtSn with TiNiSi type structure undergoes a reconstructive phase transition under 9.2 GPa at 1325 K, forming a ZrNiAl type high-pressure modification [150]. Both CePtSn phases have trivalent cerium. The two-dimensional [AuGe] polyanion in NP-CeAuGe with NdPtSb structure transforms to a three-dimensional one [157]. The TiNiSi type high-pressure modification was monitored in a diamond anvil cell and this first order transition starts at 8.7(7) GPa.

The CeT_2Sn_2 (T = Ni, Cu, Rh, Pd, Ir, Pt) stannides with tetragonal $CaBe_2Ge_2$ type structure have been studied in detail with respect to their magnetic properties [158 – 165]. The structure of $CePt_2Sn_2$ is shown as an example in Fig. 17. The platinum and tin atoms build up a three-dimensional $[Pt_2Sn_2]$ network where the platinum atoms have between four and five tin neighbours. The cerium atoms fill larger cages of coordination number 18 within this network. $CePt_2Sn_2$ shows a small range of homogeneity and exhibits a monoclinic distortion for some quenched samples [165]. Cerium is trivalent in all CeT_2Sn_2 stannides. These stannides order antiferromagnetically at Néel temperatures between 0.47 ($CeRh_2Sn_2$) and 4.1 K ($CeIr_2Sn_2$) [161]. Long-range magnetic ordering was also evident from the heat capacity measurements. Above T_N, these materials show a significant enhancement of the electronic specific heat coefficient in the order $3-4$ J/molK^2.

Another family of stannides with interesting properties are the tin-rich materials $SnRE_3T_4Sn_{12}$ [166 – 170, and ref. therein]. These stannides have a strong crystal chemical similarity with $A'A''_3B_4O_{12}$ perovskite-like ternary oxide phases with the difference, that a trigonal prismatic tin coordination is observed for the transition metal atoms instead of an octahedral one. Depending on the rare earth and transition metal components, the $SnRE_3T_4Sn_{12}$ stannides show different structural distortions which lead to superstructure formation. So far, four different phases can be distinguished. The main interest in these materials is low-temperature superconductivity. Some of these stannides show re-entrant superconductivity, others show magnetic ordering at temperatures lower than 10 K.

With manganese as transition metal component a second atom with a permanent magnetic moment can be introduced into the stannide. This has intensively been investigated for many ternary stannides $REMn_6Sn_6$ and germanides $REMn_6Ge_6$. Most investigations have been performed by the Venturini group and the crystallographic, magnetic, neutron diffraction, and Mössbauer spectroscopic data are well documented in many publications [171 – 173, and ref. therein]. Single crystals of these materials can be grown with a large excess of a gallium/indium flux. The $REMn_6Sn_6$ and $REMn_6Ge_6$ compounds show high magnetic ordering temperatures. Magnetization experiments on single crystals give detailed information on the alignment of the rare earth and manganese magnetic moments [171].

^{119}*Sn Mössbauer spectroscopy*

^{119}Sn Mössbauer spectroscopy is a useful tool for the investigation of stannides. The isomer shift gives

direct information on the *s* electron density at the tin nuclei [174 – 176]. Furthermore, in some cases it is possible to differentiate different tin species within one compound. This information can be extremely helpful for structure determination. Some interesting examples are the structures of YbAgSn [177] and $Ce_3Rh_4Sn_{13}$ [152]. Usually the isomer shifts of the intermetallic tin compounds range from 1.8 to 2.0 mm/s with respect to a $Ca^{119}SnO_3$ source. Within some series of rare earth compounds, the isomer shift can vary as a function of the electronegativity of the rare earth element. This behaviour has been studied in detail for the complete series of *RE*AuSn stannides [152, 178 – 180, and ref. therein]. For LaAuSn [178] the isomer shift is 1.85 mm/s, while ScAuSn [181] shows a much smaller value of 1.68 mm/s. This behaviour is also reflected in the ^{119}Sn solid state NMR spectra [181].

Many of the magnetically ordering rare earth metal based stannides have also been investigated by Mössbauer spectroscopy. Below the magnetic ordering temperature one can detect transferred hyperfine fields at the tin sites. Usually these fields are between 1 and 5 T, but for EuZnSn a huge hyperfine field of 12.8 T has been observed [182, 183]. Sometimes magnetic hyperfine field distributions are observed, *e. g.* in TbAuSn [180].

Hydride formation

Many of the ternary rare earth metal based stannides discussed above leave tetrahedral or other voids that can be filled by hydrogen. In recent years the groups of Yartys and Chevalier have started systematic studies of the hydrogen absorption of $RE_xT_ySn_z$ stannides and indides [184 – 187, and ref. therein]. There are two different goals when studying these materials. One is certainly the search for new hydrogen storage materials, but it is also possible to use hydrogen absorption in order to influence the physical properties of materials. This was shown for the large family of equiatomic Ce*T*Sn stannides and related compounds [187].

Besides hydrogen insertion, also lithium insertion and deinsertion was discussed for rare earth-transition metal-stannides with suitable crystal structures. A recent example is $La_3Ni_2Sn_7$ [188], where the authors claim a capacity of up to nine lithium atoms. These electrochemical studies reveal that the $RE_xT_ySn_z$ stannides might have a good potential for new electrode materials.

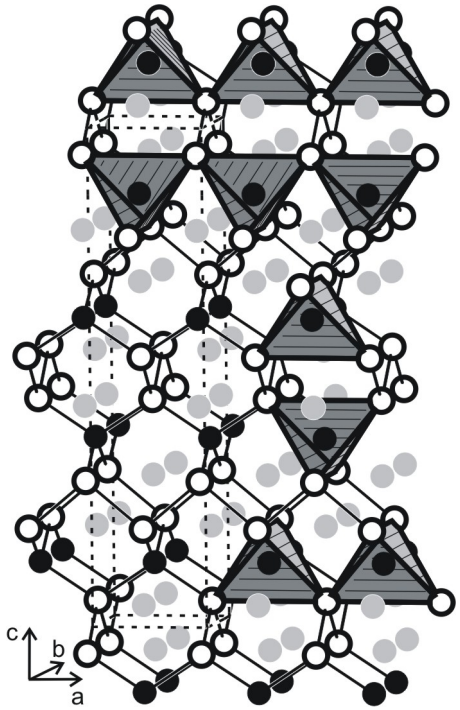

Fig. 18. The crystal structure of Li_2AuSn_2. Lithium, gold, and tin atoms are drawn as light grey, black, and open circles, respectively. The three-dimensional network of corner-sharing $AuSn_{4/2}$ tetrahedra is emphasized.

Ternary alkali and alkaline earth metal based stannides

The lithium–transition metal–tin systems have first been investigated by the groups of Schuster and Weiss, searching for new Zintl compounds and Heusler type phases [189 – 193]. They reported on several cubic phases Li_2TSn and LiT_2Sn. These stannides are particularly interesting since they exhibit intrinsic colors, *e. g.* light blue for $LiAg_2Sn$ or orange for Li_2AuSn [190]. Most studies were based on X-ray powder data and only some conductivity data were reported.

More systematic studies of the Li–*T*–Sn systems with the late transition metals were conducted in recent years with respect to the potential use of these stannides as electrode materials for battery application. Structurally remarkable compounds are $Li_{17}Ag_3Sn_6$ [194] with carbonate-like $[AgSn_3]^{11-}$ anions, the solid solutions $Li_{3-x}Pt_2Sn_{3+x}$ [195], and $LiRh_3Sn_5$ [196]. An overview on the crystal chemistry of these materials is given in [197]. Two highly interesting stannides are $LiAg_2Sn$ [198] and Li_2AuSn_2 [199]. Temperature-dependent ^{7}Li solid state NMR experiments revealed

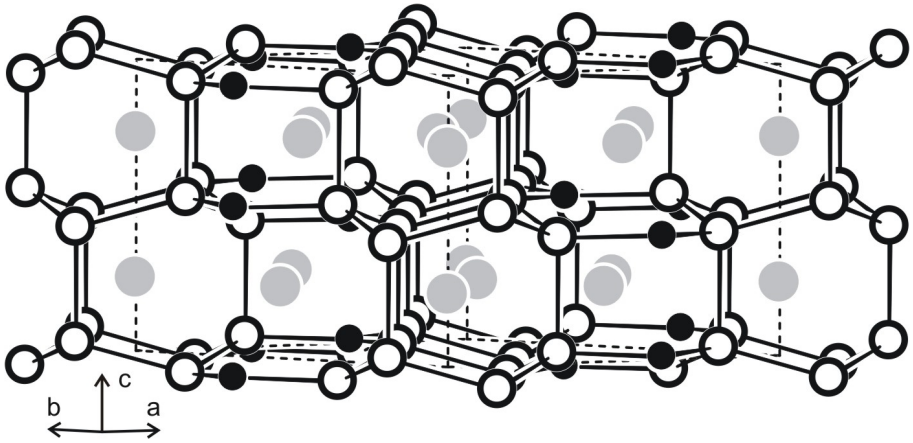

Fig. 19. The crystal structure of Na_2AuSn_3. Sodium, gold, and tin atoms are drawn as light grey, black, and open circles, respectively. The three-dimensional $[AuSn_3]$ network is emphasized.

linewidth narrowing above room temperature, indicating lithium mobility on the kHz timescale. Both stannides are mixed electronic and ionic conductors. The lithium transport in Li_2AuSn_2 proceeds through channels within a three-dimensional $[AuSn_2]$ network that is composed of condensed $AuSn_{4/2}$ tetrahedra (Fig. 18). The activation energies of lithium motion are 33 and 27 kJ/mol for $LiAg_2Sn$ and Li_2AuSn_2, respectively. Recent electrochemical experiments revealed a chemical diffusion coefficient value of 10^{-6} – 10^{-7} cm^2s^{-1} and an operating voltage range of 1.93 (± 0.02) V for $LiAg_2Sn$ [200].

The ternary systems with the heavier alkali metals sodium, potassium, rubidium, and cesium have not intensively been investigated. With sodium the stannides NaAuSn [201, 202] with TiNiSi type structure and Na_2AuSn_3 [203] with Lu_2CoGa_3 type structure have been synthesized. Both structures derive from the well known AlB_2 type by an ordered arrangement (and a puckering) of the gold and tin atoms on the boron network. An overview of the many AlB_2 superstructures is given in [204]. Equiatomic NaAuSn has exclusively Au–Sn contacts (270 – 278 pm) within its three-dimensional [AuSn] network, while Sn–Sn (294 – 297 pm), Au–Sn (270 pm) bonds, and a weak Au–Au (312 pm) contact occur in the $[AuSn_3]$ network of Na_2AuSn_3 (Fig. 19).

The tin atoms in A_3AuSn_4 (A = K, Rb, Cs) [205] form Sn_4 tetrahedra (292 – 309 pm Sn–Sn) which are bridged *via* gold atoms to one-dimensional chains that are separated and charge balanced by the alkali metal atoms. Very interesting structural units occur in the gold-rich stannide KAu_4Sn_2 [206]: $SnAu_8$ (274 – 299 pm Au–Sn) and $AuAu_4$ (270 – 302 pm Au–Au). The isotypic stannides $Rb_4Au_7Sn_2$ [207] and $Cs_4Au_7Sn_2$ [208] can be considered as substitution variants of the $MgCu_2$ type Laves phase. The three-dimensional $[Au_7Sn_2]$ networks contain $[Au_7]$ cluster units and Sn_2 dumb-bells.

With magnesium, so far only the stannides MgCuSn (cubic MgAgAs type), $MgCu_4Sn$ (ordered Laves phase) [209], $MgRuSn_4$ [210], and $Mg_2Co_3Sn_{10+x}$ [211] have been reported. These stannides show full ordering of all atomic sites. Only the $Mg_2Co_3Sn_{10+x}$ structure shows a partial occupancy of one tin site. The Ru atoms in $MgRuSn_4$ and the Co1 atoms in $Mg_2Co_3Sn_{10+x}$ have a square antiprismatic tin coordination, frequently observed for transition metal stannides. The Co2 atoms in $Mg_2Co_3Sn_{10+x}$ have trigonal prismatic tin coordination. These $Co1Sn_8$ and $Co2Sn_6$ polyhedra build up a unique three-dimensional network which leaves cavities for the magnesium atoms. It is interesting to note that solid solutions $Mg_xRh_3Sn_{7-x}$ $(x = 0.98 – 1.55)$ [210] and $Mg_xIr_3Sn_{7-x}$ $(x = 0 – 1.67)$ [16] exist, where the tin atoms are randomly substituted by magnesium. This substitution pattern has also been observed for a variety of indium intermetallics [212, and ref. therein].

With calcium, strontium, and barium several equiatomic *AET*Sn stannides with the late transition metals have been synthesized. Most of these stannides crystallize with superstructures of the AlB_2 type. For details we refer to the original work and recent reviews [204, 213 – 218].

$SrCuSn_2$ and $BaCuSn_2$ [219, 220] crystallize with the orthorhombic $CeNiSi_2$ type structure, an intergrowth structure of $ThCr_2Si_2$ and AlB_2 related slabs. Also the tin-rich stannides $SrNiSn_3$, $BaNiSn_3$, and

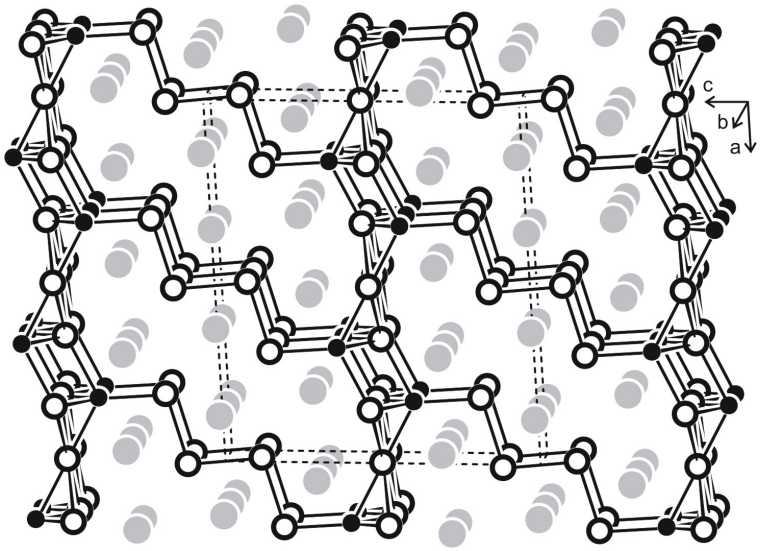

Fig. 20. The crystal structure of $Ca_6Cu_2Sn_7$. Calcium, copper, and tin atoms are drawn as light grey, black, and open circles, respectively. The tree-dimensional $[Cu_2Sn_7]$ network is emphasized.

$BaPtSn_3$ [221] belong to that family of compounds. They adopt a non-centrosymmetric, ordered version of the $ThCr_2Si_2$ type. The group-subgroup relations for the different $ThCr_2Si_2$ superstructures for $BaNiSn_3$ and other stannides are presented in [222].

The stannides $CaTSn_2$ (T = Rh, Pd, Ir) [223] crystallize with the orthorhombic $MgCuAl_2$ type and exhibit a tetrahedral tin substructure that resembles the structure of hexagonal diamond, lonsdaleite. Electronic structure calculations reveal an almost neutral tin substructure with four-bonded tin atoms for $CaRhSn_2$ and $CaIrSn_2$, while negatively charged tin centers are observed for $CaPdSn_2$ with its higher valence electron concentration. The higher *s* electron density at the tin nuclei is also reflected by the higher isomer shift in the ^{119}Sn Mössbauer spectrum. With calcium, so far, only the tin-rich stannide $Ca_2Pt_3Sn_5$ with a complex three-dimensional $[Pt_3Sn_5]$ network has been observed.

Also the stannides $Sr_3Ir_4Sn_4$ [224], $Ca_7Ni_4Sn_{13}$ [225], and $Ca_6Cu_2Sn_7$ [226] have three-dimensional networks formed by the transition metal and tin atoms with T–Sn distances close to the sums of the covalent radii. These networks leave different channels that are filled by the alkaline earth metal atoms. As an example the structure of $Ca_6Cu_2Sn_7$ is presented in Fig. 20. The copper and tin atoms build up a peculiar open three-dimensional $[Cu_2Sn_7]$ network, where two-dimensional $[Cu_2Sn_3]$ units extend in the *xy* plane around $z = 0$ and $z = 1$. These units are connected with each other *via* Sn_4 zig-zag chains, similar to the SrSn structure discussed above. Susceptibility measurements revealed Pauli paramagnetism for $Ca_7Ni_4Sn_{13}$ and $Ca_6Cu_2Sn_7$.

Uranium and thorium based stannides

The binary and ternary stannides formed by uranium and thorium often have crystal structures similar to the rare earth metal based stannides. These compounds have intensively been investigated by solid state chemists and physicists with respect to the greatly varying magnetic and electrical properties. In the U–Sn system the stannides USn_3, U_3Sn_7, USn_2, USn, and U_5Sn_4 have been reported [6, 7]. Among these stannides the magnetic structure of the 75 K antiferromagnet USn_2 (propagation vector $\mathbf{k} = 0, 0, 1/2$) has been determined on the basis of neutron powder diffraction studies [227].

The ternary systems U–T–Sn have not completely been investigated. Full phase diagram information is available for U–Fe–Sn [228] and U–Ag–Sn [229]. While the compounds U_2Fe_2Sn and UFe_5Sn have been observed in the iron system, only a solid solution UAg_xSn_{3-x} up to $x = 1$ forms in the silver based system. In several other ternary systems the equiatomic UTSn stannides occur. Among these compounds UNiSn and UPtSn crystallize with the cubic MgAgAs type; UCuSn, UPdSn and UAuSn adopt an ordered version of the $CaIn_2$ structure [230, 231], and URhSn adopts the ZrNiAl type [232]. The equiatomic UTSn stannides have intensively been studied for their magnetic properties. In most UTSn phases the tran-

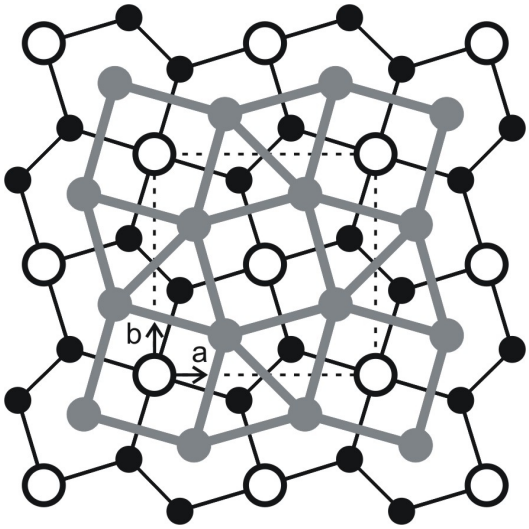

Fig. 21. The crystal structure of U_2Fe_2Sn. Uranium, iron, and tin atoms are drawn as medium grey, black, and open circles, respectively. The AlB_2 and CsCl related slabs are emphasized.

sition metal atoms do not carry a magnetic moment. In URhSn, however, a small induced moment has been observed for both crystallographically independent rhodium sites. The most investigated material in the U*T*Sn family is UNiSn. So far, more than 60 entries occur in the current SciFinder data base [8]. UNiSn is a semiconducting paramagnet at higher temperatures, but becomes a metallic antiferromagnet below the Néel temperature of *ca.* 45 K [233, 234, and ref. therein].

Several uranium stannides $UT_{2-x}Sn_{2-y}$ and UT_2Sn_2 (T = Co, Ni, Cu) crystallize with structures that derive from the $ThCr_2Si_2$ type [235–237]. Especially the magnetic properties of these stannides are interesting. UCu_2Sn_2 and UNi_2Sn_2 order antiferromagnetically below $T_N = 108$ and 35 K, respectively. For the cobalt compound a more complex magnetic behaviour with two transitions has been observed. The UT_2Sn_2 stannides have significantly higher magnetic ordering temperatures than the corresponding cerium compounds.

A large number of uranium intermetallics crystallizes with the Mo_2FeB_2 structure, a simple intergrowth variant of distorted CsCl and AlB_2 related slabs. U_2Fe_2Sn and U_2Rh_2Sn were the first stannides in that particular series of materials [238]. As an example we present the U_2Fe_2Sn structure in Fig. 21. The uranium atoms build up the trigonal and square prisms that are filled by the iron and tin atoms, respectively. Since the trigonal prisms are condensed *via* rectangular faces, one observes Fe_2 dumb-bells with an Fe–Fe distance of 273 pm. This family of compounds has intensively been investigated in the last ten years and the studies have been extended to neptunium, plutonium, and americium as actinoid components. Now the stannides U_2T_2Sn (T = Fe, Co, Ni, Ru, Rh, Pd, Ir, Pt), Np_2T_2Sn (T = Co, Ni, Ru, Rh, Pd, Pt), Pu_2T_2Sn (T = Ni, Pd, Pt), and Am_2T_2Sn (T = Ni, Pd) are known. The crystallographic and magnetic data of these exciting materials are summarized in a recent review [239]. Among the uranium based stannides the 15 K antiferromagnet U_2Pt_2Sn shows the highest electronic specific heat coefficient γ of 327 mJ/molK^2. The magnetic ordering of the neptunium stannides could nicely be monitored *via* ^{237}Np Mössbauer spectroscopy and a complete bonding analyses of the Np_2T_2Sn stannides was performed from density functional calculations [240].

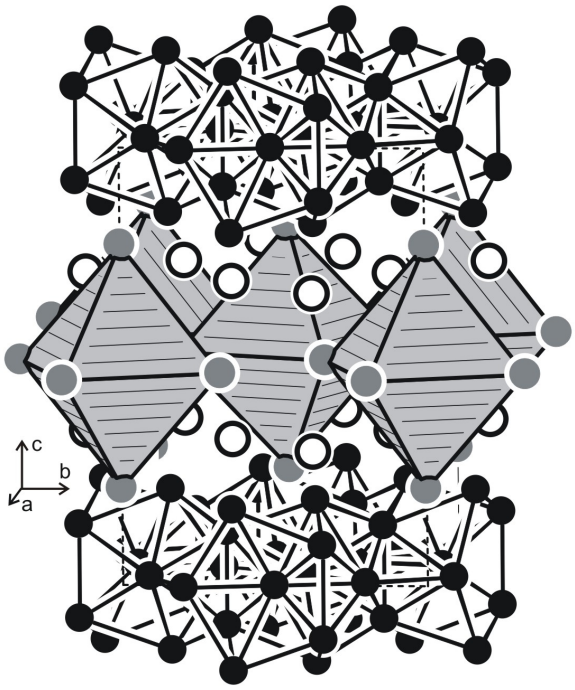

Fig. 22. The crystal structure of $Th_4Fe_{13}Sn_5$. Thorium, iron, and tin atoms are drawn as medium grey, black, and open circles, respectively. The two-dimensional iron substructure and the condensed $SnTh_6$ octahedra are emphasized.

With thorium as the actinoid component, the Th–Fe–Sn system has systematically been studied, leading to the stannides $Th_4Fe_{13}Sn_5$ with a new structure type and $ThFe_{0.22}Sn_2$ with a defect $CeNiSi_2$ structure

[241 – 243]. This is different from the cobalt and nickel system, where MgAgAs type ThNiSn and ZrNiAl type ThCoSn occur, similar to the uranium based systems.

$Th_4Fe_{13}Sn_5$ exhibits a remarkable structure (Fig. 22). One observes a clear segregation. The iron atoms build up a two-dimensional network around $z = 0$ and $z = 1$ that is separated by a thorium stannide slab in which the Sn2 atoms have octahedral thorium coordination. Within the Fe_{13} cluster the Fe–Fe distances range from 243 to 268 pm and the Sn1 atoms are connected to the cluster unit *via* short Fe–Sn contacts of 256 and 277 pm. The Fe_{13} cluster is magnetic. $Th_4Fe_{13}Sn_5$ orders ferromagnetically at 375 K as is evident from magnetization and ^{57}Fe Mössbauer spectroscopic experiments. Transferred hyperfine fields can be detected at the tin nuclei. In contrast, the iron-poor stannide $ThFe_{0.22}Sn_2$ does not order magnetically.

Outlook

Stannides find broad application in various fields of technology and in daily life. The different facets of stannide chemistry have been reviewed herein. The many new publications that appear every year manifest the actuality of this vivid field of research and one can certainly expect innovative applications of stannides in the near future. Often it takes some time from the synthesis of a material to its application. An example is ZrNiSn which was first synthesized by Wolfgang Jeitschko in 1970 and had its thermoelectric properties investigated only recently.

Acknowledgements

I am indebted to Dipl.-Chem. F. M. Schappacher and Th. Fickenscher for the scanning electron micrographs and the molten tin bars and to Prof. U. Häussermann for supplying the Ir_3Sn_7 crystals. This work was supported by the Deutsche Forschungsgemeinschaft.

[1] J. Donohue, The Structures of the Elements, Wiley, New York (1974).
[2] Holleman-Wiberg, N. Wiberg (ed.), Lehrbuch der Anorganischen Chemie, de Gruyter, 101. Aufl., Berlin (1995).
[3] H. Bärnighausen, Commun. Math. Chem. **9**, 139 (1980).
[4] http://www.theodoregray.com/PeriodicTable/Elements/050/
[5] C. J. Evans, Tin Handbook, 3rd ed., Hüthig, Heidelberg (1994).
[6] T. B. Massalski, Binary Alloy Phase Diagrams. American Society for Metals, Metals Park, Ohio 44073 (1986).
[7] P. Villars, L. D. Calvert, Pearson's Handbook of Crystallographic Data for Intermetallic Phases, 2nd ed., American Society for Metals, Materials Park, OH 44073, (1991); and desk edition (1997).
[8] SciFinder Scholar version 2005: http://www.cas.org/SCIFINDER/SCHOLAR/
[9] J. Emsley, The Elements, Oxford University Press, Oxford (1999).
[10] R. Pöttgen, Th. Gulden, A. Simon, GIT Labor Fachzeitschrift **43**, 133 (1999).
[11] D. Kußmann, R.-D. Hoffmann, R. Pöttgen, Z. Anorg. Allg. Chem. **624**, 1727 (1998).
[12] R. Pöttgen, A. Lang, R.-D. Hoffmann, B. Künnen, G. Kotzyba, R. Müllmann, B. D. Mosel, C. Rosenhahn, Z. Kristallogr. **214**, 143 (1999).
[13] J. D. Corbett, Inorg. Synth. **22**, 15 (1983).
[14] P. Jolibois, C. R. Hebd. Séances Acad. Sci. **150**, 106 (1910).
[15] M. G. Kanatzidis, R. Pöttgen, W. Jeitschko, Angew. Chem. **117**, 7156 (2005); Angew. Chem. Int. Ed. **44**, 6996 (2005).
[16] M. Schlüter, U. Häussermann, B. Heying, R. Pöttgen, J. Solid State Chem. **173**, 418 (2003).
[17] B. M. Leonard, N. S. P. Bhuvanesh, R. E. Schaak, J. Am. Chem. Soc. **127**, 7326 (2005).
[18] S. Lange, T. Nilges, R.-D. Hoffmann, R. Pöttgen, Z. Anorg. Allg. Chem., in press.
[19] Ch. Xu, Y.-L. Tsai, B. E. Koel, J. Phys. Chem. **98**, 585 (1994).
[20] M. Rehbein, R. D. Fischer, M. Epple, Thermochim. Acta **382**, 143 (2002).
[21] A. K. Ganguli, A. M. Guloy, E. A. Leon-Escamilla, J. D. Corbett, Inorg. Chem. **32**, 4349 (1993).
[22] J. T. Vaughey, J. D. Corbett, Inorg. Chem. **36**, 4316 (1997).
[23] T. F. Fässler, C. Kronseder, Angew. Chem. **109**, 2800 (1997); Angew. Chem. Int. Ed. Engl. **36**, 2683 (1997).
[24] T. F. Fässler, C. Kronseder, Angew. Chem. **110**, 1641 (1998).
[25] T. F. Fässler, S. Hoffmann, Z. Anorg. Allg. Chem. **626**, 106 (2000).
[26] F. Zürcher, R. Nesper, S. Hoffmann, T. F. Fässler, Z. Anorg. Allg. Chem. **627**, 2211 (2001).
[27] T. F. Fässler, S. Hoffmann, C. Kronseder, Z. Anorg. Allg. Chem. **627**, 2486 (2001).
[28] C. Lupu, J.-G. Mao, J. W. Rabalais, A. M. Gu-

loy, J. W. Richardson (Jr.), Inorg. Chem. **42**, 3765 (2003).
[29] T. F. Fässler, S. Hoffmann, Inorg. Chem. **42**, 5474 (2003).
[30] S. Hoffmann, T. F. Fässler, Inorg. Chem. **42**, 8748 (2003).
[31] A. Palenzona, M. Pani, J. Alloys Compd. **384**, 227 (2004).
[32] F. Dubois, M. Schreyer, T. F. Fässler, Inorg. Chem. **44**, 477 (2005).
[33] S. Gupta, A. K. Ganguli, Inorg. Chem. **44**, 7443 (2005).
[34] F. Dubois, T. F. Fässler, J. Am. Chem. Soc. **127**, 3264 (2005).
[35] D. A. Hansen, L. J. Chang, Acta Crystallogr. **B25**, 2392 (1969).
[36] W. Müller, H. Schäfer, Z. Naturforsch. **28b**, 246 (1973).
[37] W. Müller, Z. Naturforsch. **29b**, 304 (1974).
[38] U. Frank, W. Müller, H. Schäfer, Z. Naturforsch. **30b**, 1 (1975).
[39] U. Frank, W. Müller, Z. Naturforsch. **30b**, 316 (1975).
[40] G. R. Goward, N. J. Taylor, D. C. S. Souza, L. F. Nazar, J. Alloys Compd. **329**, 82 (2001).
[41] R. Nesper, Prog. Solid State Chem. **20**, 1 (1990).
[42] M. Winter, J. O. Besenhard, Electrochim. Acta **45**, 31 (1999).
[43] R. A. Huggins, in J. O. Besenhard (ed.): Handbook of Battery Materials, Wiley–VCH, Weinheim (1999).
[44] R. A. Dunlap, D. A. Small, D. D. MacNeil, M. N. Obrovac, J. R. Dahn, J. Alloys Compd. **289**, 135 (1999).
[45] R. A. Dunlap, O. Mao, J. R. Dahn, Phys. Rev. B **59**, 3494 (1999).
[46] P. E. Lippens, J.-C. Jumas, J. Olivier-Fourcade, Hyp. Int. **156/157**, 327 (2004).
[47] F. Yin, X. Su, Zh. Li, J. Wang, J. Alloys Compd. **393**, 105 (2005).
[48] O. Genser, J. Hafner, Phys. Rev. B **63**, 144204 (2001).
[49] T. F. Fässler, S. Hoffmann, Z. Kristallogr. **214**, 722 (1999).
[50] H. G. von Schnering, R. Kroner, M. Baitinger, K. Peters, R. Nesper, Yu. Grin, Z. Kristallogr.-NCS **215**, 205 (2000).
[51] G. S. Nolas, T. J. R. Weakly, J. L. Cohn, Chem. Mater. **11**, 2470 (1999).
[52] G. S. Nolas, B. C. Chakoumakos, B. Mahieu, G. J. Long, T. J. R. Weakly, Chem. Mater. **12**, 1947 (2000).
[53] G. S. Nolas, J. L. Cohn, J. S. Dyck, C. Uher, J. Yang, Phys. Rev. B **65**, 165201 (2002).
[54] Yu. Grin, M. Baitinger, R. Kniep, H. G. von Schnering, Z. Kristallogr.-NCS **214**, 453 (1999).
[55] M. Baitinger, Yu. Grin, R. Kniep, H. G. von Schnering, Z. Kristallogr.-NCS **214**, 457 (1999).
[56] C. Hoch, M. Wendorf, C. Röhr, Acta Crystallogr. **C58**, i45 (2002).
[57] C. Hoch, M. Wendorf, C. Röhr, Z. Anorg. Allg. Chem. **628**, 2172 (2002).
[58] C. Hoch, M. Wendorf, C. Röhr, J. Alloys Compd. **361**, 206 (2003).
[59] C. Hoch, M. Wendorf, C. Röhr, Z. Anorg. Allg. Chem. **629**, 2391 (2003).
[60] H. Schäfer, B. Eisenmann, W. Müller, Angew. Chem. **85**, 742 (1973).
[61] G. H. Grosch, K.-J. Range, J. Alloys Compd. **235**, 250 (1996).
[62] A. Widera, H. Schäfer, J. Less-Common Met. **77**, 29 (1981).
[63] S. M. Kauzlarich (ed.): Chemistry, Structure, and Bonding of Zintl Phases and Ions, VCH, Weinheim (1996).
[64] A. Palenzona, P. Manfrinetti, M. L. Fornasini, J. Alloys Compd. **280**, 211 (1998).
[65] P. Manfrinetti, D. Mazzone, A. Palenzona, J. Alloys Compd. **284**, L1 (1999).
[66] S. Bobev, S. C. Sevov, J. Alloys Compd. **338**, 87 (2002).
[67] S. Bobev, S. C. Sevov, Inorg. Chem. **40**, 5361 (2001).
[68] I. Todorov, S. C. Sevov, Inorg. Chem. **43**, 6490 (2004).
[69] S. Bobev, S. C. Sevov, Inorg. Chem. **39**, 5930 (2000).
[70] I. Todorov, S. C. Sevov, Inorg. Chem. **44**, 5361 (2005).
[71] S. Bobev, S. C. Sevov, Angew. Chem. Int. Ed. **39**, 4108 (2000).
[72] B. D. McWhan, P. C. Souers, G. Jura, Phys. Rev. **143**, 385 (1966).
[73] B. Stroka, J. Wosnitza, E. Scheer, H. von Löhneysen, W. Park, K. Fischer, Z. Phys. Condens. Matter **89**, 39 (1992).
[74] W. Müller, R. Voltz, Z. Naturforsch. **29b**, 163 (1974).
[75] R. Türck, H. Kalpen, K. Peters, H. G. von Schnering, Z. Kristallogr. **Suppl. 9**, 234 (1995).
[76] R. Türck, Untersuchungen an inversen Perowskiten M_3SiO, M_3GeO, Eu_3YO (M = Ca, Sr, Ba, Eu; Y = Sn, Pb) und an neuen ternären Alkalimetallzinkpnictiden MZn_4Y_3 und $K_2Zn_5Y_4$ (M = Na, K, Rb, Cs; Y = P, As). Dissertation, Universität Stuttgart, 1994.
[77] G. Frisch, C. Hoch, C. Röhr, P. Zönnchen, K.-D. Becker, D. Niemeier, Z. Anorg. Allg. Chem. **629**, 1661 (2003).
[78] R. Eger, Hj. Mattausch, A. Simon, Z. Naturforsch. **48b**, 48 (1993).
[79] E. A. Leon-Escamilla, J. D. Corbett, Inorg. Chem. **40**, 1226 (2001).
[80] J. D. Corbett, E. A. Leon-Escamilla, J. Alloys Compd. **356 – 357**, 59 (2003).
[81] B. Huang, J. D. Corbett, Inorg. Chem. **36**, 3730 (1997).
[82] M. Mathon, M. Gambino, E. Hayer, M. Gaune-Escard, J. P. Bros, J. Alloys Compd. **285**, 123 (1999).

[83] B. Künnen, W. Jeitschko, G. Kotzyba, B. D. Mosel, Z. Naturforsch. **55b**, 425 (2000).
[84] H. Kleinke, M. Waldeck, P. Gütlich, Chem. Mater. **12**, 2219 (2000).
[85] Y.-U. Kwon, J. D. Corbett, Chem. Mater. **2**, 27 (1990).
[86] T. Wölpl, W. Jeitschko, J. Alloys Compd. **210**, 185 (1994).
[87] T. Wölpl, W. Jeitschko, Z. Anorg. Allg. Chem. **620**, 467 (1994).
[88] U. Häussermann, S. I. Simak, I. A. Abrokosov, B. Johansson, S. Lidin, J. Am. Chem. Soc. **120**, 10136 (1998).
[89] F. C. Frank, J. S. Kasper, Acta Crystallogr. **11**, 184 (1958).
[90] F. C. Frank, J. S. Kasper, Acta Crystallogr. **12**, 483 (1959).
[91] J. Etourneau, Superconducting Materials, in A. K. Cheetham, P. Day (ed.): Solid State Chemistry – Compounds, Chapter 3, Clarendon Press, Oxford (1992).
[92] M. Elding-Pontén, L. Stenberg, S. Lidin, G. Madariaga, J.-M. Pérez-Mato, Acta Crystallogr. B **53**, 364 (1997).
[93] A. Leineweber, O. Oeckler, U. Zachwieja, J. Solid State Chem. **177**, 936 (2004).
[94] A. Leineweber, J. Solid State Chem. **177**, 1197 (2004).
[95] A. L. Lyubimtsev, A. I. Baranov, A. Fischer, L. Kloo, B. A. Popovkin, J. Alloys Compd. **340**, 167 (2002).
[96] A. Lang, W. Jeitschko, J. Mater. Chem. **6**, 1897 (1996).
[97] B. Künnen, D. Niepmann, W. Jeitschko, J. Alloys Compd. **309**, 1 (2000).
[98] U. Häussermann, A. Landa-Cánovas, S. Lidin, Inorg. Chem. **36**, 4307 (1997).
[99] A. Lang, W. Jeitschko, Z. Metallkd. **87**, 759 (1996).
[100] J. Nylén, F. J. Garcìa Garcìa, B. D. Mosel, R. Pöttgen, U. Häussermann, Solid State Sci. **6**, 147 (2004).
[101] P. Sreeraj, R.-D. Hoffmann, Zh. Wu, R. Pöttgen, U. Häussermann, Chem. Mater. **17**, 911 (2005).
[102] G. Y. Li, Y. C. Chan, J. Electron. Packaging **124**, 305 (2002).
[103] H. D. Blair, T.-Yu. Pab, J. M. Nicholson, in: Proceedings of the 48th Electronic Components and Technology Conference, Dearborn, MI, 259 (1998).
[104] G. Gosh, J. Electr. Mater. **28**, 1238 (1999).
[105] Y.-Ch. Hsu, Y.-M. Huang, Ch. Chen, H. Wang, J. Alloys Compd. (2006), in press.
[106] C. Luef, A. Paul, H. Flandorfer, A. Kodentsov, H. Ipser, J. Alloys Compd. **391**, 67 (2005).
[107] P. Claus, M. Lucas, K. Schrödter, Chem.-Ing. Tech. **65**, 569 (1993).
[108] Th. F. Fässler, in: 225th ACS National Meeting, New Orleans, LA, abstract INOR-093 (2003).
[109] Z. Karpinski, J. Clarke, J. Chem. Soc. Faraday Trans. II **71**, 893 (1975).
[110] B. H. Davis, J. Catal. **46**, 348 (1977).
[111] G. Meitzner, G. H. Via, F. W. Lytle, S. C. Fung, J. H. Sinfelt, J. Phys. Chem. **92**, 2925 (1988).
[112] Ch. Xu, B. E. Koel, Surf. Sci. **304**, 249 (1994).
[113] Ch. Xu, J. W. Peck, B. E. Koel, J. Am. Chem. Soc. **115**, 751 (1993).
[114] M. T. Paffett, R. G. Windham, Surf. Sci. **208**, 34 (1989).
[115] L. S. Carvalho, C. L. Pieck, M. C. Rangel, N. S. Fígoli, C. R. Vera, J. M. Parera, Appl. Catal. A: General **269**, 105 (2004).
[116] C. Carnevillier, F. Epron, P. Marécot, Appl. Catal. A: General **275**, 25 (2004).
[117] L. S. Carvalho, C. L. Pieck, M. C. Rangel, N. S. Fígoli, J. M. Grau, P. Reyes, J. M. Parera, Appl. Catal. A: General **269**, 91 (2004).
[118] F. Epron, C. Carnevillier, P. Marécot, Appl. Catal. A: General **295**, 157 (2005).
[119] Y. Pouilloux, F. Autin, A. Piccirilli, C. Guimon, J. Barrault, Appl. Catal. A: General **169**, 65 (1998).
[120] X.-Q. Cheng, P.-F. Shi, J. Alloys Compd. **391**, 241 (2005).
[121] J. Yin, M. Wada, S. Yoshida, K. Ishihara, S. Tanase, T. Sakai, J. Electrochem. Soc. **150**, A1129 (2003).
[122] M. Wachtler, M. Winter, J. O. Besenhard, J. Power Sources **105**, 151 (2002).
[123] R. Benedek, M. M. Thackeray, J. Power Sources **110**, 406 (2002).
[124] J. O. Besenhard, J. Yang, M. Winter, J. Power Sources **68**, 87 (1997).
[125] J. Yang, M. Winter, J. O. Besenhard, Solid State Ionics **90**, 281 (1996).
[126] K. D. Kepler, J. T. Vaughey, M. M. Thackeray, Electrochem. Solid-State Lett. **2**, 307 (1999).
[127] M. M. Thackeray, J. T. Vaughey, A. J. Kahaian, K. D. Kepler, R. Benedek, Electrochem. Commun. **1**, 111 (1999).
[128] D. Larcher, L. Y. Beaulieu, D. D. MacNeil, J. R. Dahn, J. Electrochem. Soc. **147**, 1658 (2000).
[129] L. Zavalij, A. Zribi, R. R. Chromik, S. Pitely, P. Y. Zavalij, E. J. Cotts, J. Alloys Compd. **334**, 79 (2002).
[130] A. Neumann, A. Kjekshus, E. Røst, J. Solid State Chem. **123**, 203 (1996).
[131] A. V. Tkachuk, L. G. Akselrud, Yu. V. Stadnyk, O. I. Bodak, J. Alloys Compd. **312**, 284 (2000).
[132] L. Offerns, A. Neumann Torgersen, A. Kjekshus, J. Alloys Compd. **307**, 174 (2000).
[133] A. Neumann, L. Offerns, A. Kjekshus, B. Klewe, J. Alloys Compd. **274**, 136 (1998).
[134] L. Offerns, A. Neumann Torgersen, H. W. Brinks, A. Kjekshus, B. Hauback, J. Alloys Compd. **288**, 117 (1999).
[135] J. F. Roeder, M. R. Notis, J. I. Goldstein, Defects Diffus. Forum **59**, 271 (1988).
[136] W. Jeitschko, Metall. Trans. AIME **1**, 3159 (1970).

[137] S. Katsuyama, H. Matsushima, M. Ito, J. Alloys Compd. **385**, 232 (2004).
[138] C. Uher, J. Yang, S. Hu, D. T. Morelli, G. P. Meisner, Phys. Rev. B **59**, 8615 (1999).
[139] J. Tobola, J. Pierre, S. Kaprzyk, R. V. Skolozdra, M. A. Kouacou, J. Magn. Magn. Mater. **159**, 192 (1996).
[140] M. G. Shelyapina, N. Koblyuk, L. Romaka, Yu. Stadnyk, O. Bodak, E. K. Hlil, P. Wolfers, D. Fruchart, J. Toboła, J. Alloys Compd. **347**, 43 (2002).
[141] Y.-U. Kwon, J. D. Corbett, Chem. Mater. **4**, 187 (1992).
[142] M. Armbrüster, P. Simon, Yu. Grin, Z. Anorg. Allg. Chem. **630**, 1702 (2004).
[143] R. Pöttgen, R.-D. Hoffmann, unpublished results.
[144] H. Hillebrecht, M. Ade, Z. Anorg. Allg. Chem. **625**, 572 (1999).
[145] W. Reichelt, T. Söhnel, O. Rademacher, H. Oppermann, A. Simon, J. Köhler, Hj. Mattausch, Angew. Chem. **107**, 2307 (1995); Angew. Chem. Int. Ed. Engl. **34**, 2113 (1995).
[146] T. Söhnel, W. Reichelt, Acta Crystallogr. **C53**, 9 (1997).
[147] T. Söhnel, P. Böttcher, W. Reichelt, F. E. Wagner, Z. Anorg. Allg. Chem. **624**, 708 (1998).
[148] T. Söhnel, Z. Anorg. Allg. Chem. **630**, 1759 (2004).
[149] R. V. Skolozdra, Stannides of the rare-earth and transition metals, in K. A. Gschneidner (Jr.), L. Eyring: Handbook on the Physics and Chemistry of Rare Earths, Vol. 24, chapter 164, Elsevier, Amsterdam (1997).
[150] J. F. Riecken, G. Heymann, T. Soltner, R.-D. Hoffmann, H. Huppertz, D. Johrendt, R. Pöttgen, Z. Naturforsch. **60b**, 821 (2005).
[151] T. Schmidt, D. Johrendt, C. P. Sebastian, R. Pöttgen, K. Łątka, R. Kmieć, Z. Naturforsch. **60b**, 1036 (2005).
[152] D. Niepmann, R. Pöttgen, K. M. Poduska, F. J. DiSalvo, H. Trill, B. D. Mosel, Z. Naturforsch. **56b**, 1 (2001).
[153] R. V. Skolozdra, L. P. Komarovskaya, O. E. Terletskaya, L. G. Akselrud, Kristallografiya **36**, 492 (1991).
[154] A. Szytuła, J. Leciejewicz, Handbook of Crystal Structures and Magnetic Properties of Rare Earth Intermetalliocs, CRC Press, Boca Raton (1994).
[155] T. Fujita, T. Suzuki, S. Nishigori, T. Takabatake, H. Fujii, J. Sakurai, J. Magn. Magn. Mater. **108**, 35 (1992).
[156] A. Ślebarski, M. B. Maple, E. J. Freeman, C. Sirvent, M. Radłowska, A. Jezierski, E. Granado, Q. Huang, J. W. Lynn, Phil. Mag. B **82**, 943 (2002).
[157] V. Brouskov, M. Hanfland, R. Pöttgen, U. Schwarz, Z. Kristallogr. **220**, 122 (2005).
[158] M. Selsane, M. Lebail, N. Hamdaoui, J. P. Kappler, H. Noël, J. C. Achard, C. Godart, Physica B **163**, 213 (1990).
[159] M. Selsane, J. C. Achard, C. Godart, W. P. Beyermann, M. F. Hundley, P. C. Canfield, J. L. Smith, J. D. Thompson, N. Hamdaoui, J. P. Kappler, Eur. J. Solid State Inorg. Chem. **28**, 567 (1991).
[160] W. P. Beyermann, M. F. Hundley, P. C. Canfield, C. Godart, M. Selsane, Z. Fisk, J. L. Smith, J. D. Thompson, Physica B **171**, 373 (1991).
[161] W. P. Beyermann, M. F. Hundley, P. C. Canfield, J. D. Thompson, M. Latroche, C. Godart, M. Selsane, Z. Fisk, J. L. Smith, Phys. Rev. B **43**, 13130 (1991).
[162] E. Lidström, A. M. Ghandour, L. Häggström, Y. Andersson, J. Alloys Compd. **232**, 95 (1996).
[163] A. Ślebarski, A. Jezierski, A. Zygmunt, M. Neumann, S. Mähl, G. Borstel, J. Magn. Magn. Mater. **159**, 179 (1996).
[164] J. Sakurai, H. Takagi, T. Kuwai, Y. Isikawa, J. Magn. Magn. Mater. **177 – 181**, 407 (1998).
[165] H.-P. Liu, M. Colarieti-Tosti, A. Broddefalk, Y. Andersson, E. Lidström, O. Eriksson, J. Alloys Compd. **306**, 30 (2000).
[166] J. L. Hodeau, J. Chenavas, M. Marezio, J. P. Remeika, Solid State Commun. **36**, 839 (1980).
[167] J. P. Remeika, G. P. Espinosa, A. S. Cooper, H. Barz, J. M. Rowell, D. B. McWhan, J. M. Vandenberg, D. E. Moncton, Z. Fisk, L. D. Woolf, H. C. Hamaker, M. B. Maple, G. Shirane, W. Thomlinson, Solid State Commun. **34**, 923 (1980).
[168] G. P. Espinosa, A. S. Cooper, H. Barz, Mater. Res. Bull. **17**, 963 (1982).
[169] J. L. Hodeau, M. Marezio, J. P. Remeika, C. H. Chen, Solid State Commun. **42**, 97 (1982).
[170] S. Miraglia, J. L. Hodeau, M. Marezio, C. Laviron, M. Ghedira, G. P. Espinosa, J. Solid State Chem. **63**, 358 (1986).
[171] L. Zhang, J. C. P. Klaasse, E. Brück, K. H. J. Buschow, F. R. de Boer, S. Yoshii, K. Kindo, C. Lefèvre, G. Venturini, Phys. Rev. B **70**, 224425 (2004).
[172] F. Canepa, R. Duraj, C. Lefèvre, B. Malaman, A. Mar, T. Mazet, M. Napoletano, A. Szytuła, J. Tobola, G. Venturini, A. Vernière, J. Alloys Compd. **383**, 10 (2004).
[173] G. Venturini, J. Alloys Compd. **398**, 42 (2005).
[174] M. Cordey-Hayes, J. Inorg. Nucl. Chem. **26**, 915 (1964).
[175] M. Cordey Hayes, I. R. Harris, Phys. Lett. **24A**, 80 (1967).
[176] M. Cordey Hayes, ^{119m}Sn: Inorganic Compounds, Metals, Alloys, in V. I. Goldanskii, R. H. Herber: Chemical Applications of Mössbauer Spectroscopy, Academic Press, New York (1968).
[177] R. Pöttgen, P. E. Arpe, C. Felser, D. Kußmann, R. Müllmann, B. D. Mosel, B. Künnen, G. Kotzyba, J. Solid State Chem. **145**, 668 (1999).
[178] K. Łątka, W. Chajek, R. Kmieć, A. W. J. Pacyna, J. Magn. Magn. Mater. **224**, 241 (2001).

[179] D. Bialic, R. Kruk, R. Kmieć, K. Tomala, J. Alloys Compd. **257**, 49 (1997).
[180] K. Łątka, J. Gurgul, R. Kmieć, A. W. Pacyna, J. Alloys Compd. **400**, 16 (2005).
[181] C. P. Sebastian, H. Eckert, S. Rayaprol, R.-D. Hoffmann, R. Pöttgen, Solid State Sci., in press.
[182] U. Ernet, R. Müllmann, B. D. Mosel, H. Eckert, R. Pöttgen, G. Kotzyba, J. Mater. Chem. **7**, 255 (1997).
[183] R. Müllmann, U. Ernet, B. D. Mosel, H. Eckert, R. K. Kremer, R.-D. Hoffmann, R. Pöttgen, J. Mater. Chem. **11**, 1133 (2001).
[184] M. Sato, M. Stange, J. P. Maehlen, V. A. Yartys, J. Alloys Compd. **397**, 165 (2005).
[185] T. Spataru, G. Principi, V. Kuncser, W. Keune, V. A. Yartys, J. Alloys Compd. **366**, 81 (2004).
[186] B. Chevalier, J.-L. Bobet, M. Pasturel, E. Bauer, F. Weill, R. Decourt, J. Etourneau, Chem. Mater. **15**, 2181 (2003).
[187] J.-L. Bobet, M. Pasturel, B. Chevalier, Intermetallics **14**, 544 (2006).
[188] S. Matsuno, T. Kohno, N. Takami, F. Kawashima, T. Sawa, Electrochem. Solid-State Lett. **8**, A234 (2005).
[189] H. Pauly, A. Weiss, H. Witte, Z. Metallkd. **59**, 47 (1968).
[190] H.-U. Schuster, D. Thiedemann, H. Schönemann, Z. Anorg. Allg. Chem. **370**, 160 (1969).
[191] C.-J. Kistrup, H.-U. Schuster, Z. Anorg. Allg. Chem. **410**, 113 (1974).
[192] U. Eberz, W. Seelentag, H.-U. Schuster, Z. Naturforsch. **35b**, 1341 (1980).
[193] J. Drews, U. Eberz, H.-U. Schuster, J. Less-Common Met. **116**, 271 (1986).
[194] C. Lupu, C. Downie, A. M. Guloy, T. A. Albright, J.-G. Mao, J. Am. Chem. Soc. **126**, 4386 (2004).
[195] R.-D. Hoffmann, Zh. Wu, R. Pöttgen, Eur. J. Inorg. Chem. 3425 (2003).
[196] P. Sreeraj, D. Johrendt, H. Müller, R.-D. Hoffmann, Zh. Wu, R. Pöttgen, Z. Naturforsch. **60b**, 933 (2005).
[197] R. Pöttgen, Zh. Wu, R.-D. Hoffmann, G. Kotzyba, H. Trill, J. Senker, D. Johrendt, B. D. Mosel, H. Eckert, Heteroatom Chem. **13**, 506 (2002).
[198] Zh. Wu, R.-D. Hoffmann, D. Johrendt, B. D. Mosel, H. Eckert, R. Pöttgen, J. Mater. Chem. **13**, 2561 (2003).
[199] Zh. Wu, B. D. Mosel, H. Eckert, R.-D. Hoffmann, R. Pöttgen, Chem. Eur. J. **10**, 1558 (2004).
[200] P. Sreeraj, H.-D. Wiemhöfer, R.-D. Hoffmann, J. Walter, A. Kirfel, R. Pöttgen, Solid State Sci., submitted for publication.
[201] G. Wrobel, H.-U. Schuster, Z. Anorg. Allg. Chem. **432**, 95 (1977).
[202] G. Nuspl, K. Polborn, J. Evers, G. A. Landrum, R. Hoffmann, Inorg. Chem. **35**, 6922 (1996).
[203] U. Zachwieja, Z. Anorg. Allg. Chem. **627**, 353 (2001).
[204] R.-D. Hoffmann, R. Pöttgen, **216**, 127 (2001).
[205] U. Zachwieja, J. Müller, J. Wlodarski, Z. Anorg. Allg. Chem. **624**, 853 (1998).
[206] H.-D. Sinnen, H.-U. Schuster, Z. Naturforsch. **33b**, 1077 (1978).
[207] H.-D. Sinnen, H.-U. Schuster, Z. Naturforsch. **36b**, 833 (1981).
[208] U. Zachwieja, J. Wlodarski, Z. Anorg. Allg. Chem. **624**, 1443 (1998).
[209] K. Osamura, Y. Murakami, J. Less-Common Met. **60**, 311 (1978).
[210] M. Schlüter, A. Kunst, R. Pöttgen, Z. Anorg. Allg. Chem. **628**, 2641 (2002).
[211] M. Schreyer, G. Kraus, T. F. Fässler, Z. Anorg. Allg. Chem. **630**, 2520 (2004).
[212] V. Hlukhyy, U. Ch. Rodewald, Z. Anorg. Allg. Chem. **631**, 2997 (2005).
[213] F. Merlo, M. Pani, M. L. Formasini, J. Less-Common Met. **171**, 329 (1991).
[214] F. Merlo, M. Pani, M. L. Fornasini, J. Alloys Compd. **196**, 145 (1993).
[215] F. Merlo, M. Pani, M. L. Fornasini, J. Alloys Compd. **232**, 289 (1996).
[216] R.-D. Hoffmann, R. Pöttgen, D. Kußmann, D. Niepmann, H. Trill, B. D. Mosel, Solid State Sci. **4**, 481 (2002).
[217] M. D. Bojin, R. Hoffmann, Helv. Chim. Acta **86**, 1653 (2003).
[218] M. D. Bojin, R. Hoffmann, Helv. Chim. Acta **86**, 1683 (2003).
[219] N. May, H. Schäfer, Z. Naturforsch. **29b**, 20 (1974).
[220] W. Dörrscheidt, G. Savelsberg, J. Stöhr, H. Schäfer, J. Less-Common Met. **83**, 269 (1982).
[221] W. Dörrscheidt, H. Schäfer, J. Less-Common Met. **58**, 209 (1978).
[222] D. Kußmann, R. Pöttgen, U. Ch. Rodewald, C. Rosenhahn, B. D. Mosel, G. Kotzyba, B. Künnen, Z. Naturforsch. **54b**, 1155 (1999).
[223] R.-D. Hoffmann, D. Kußmann, U. Ch. Rodewald, R. Pöttgen, C. Rosenhahn, B. D. Mosel, Z. Naturforsch. **54b**, 709 (1999).
[224] R.-D. Hoffmann, D. Kußmann, R. Pöttgen, Int. J. Inorg. Mater. **2**, 135 (2000).
[225] D. A. Vennos, M. E. Badding, F. J. DiSalvo, J. Less-Common Met. **175**, 339 (1991).
[226] Z.-M. Sun, S.-Q. Xia, Y.-Z. Huang, L.-M. Wu, J.-G. Mao, Inorg. Chem. **44**, 9242 (2005).
[227] P. Boulet, G. André, F. Bourée, H. Noël, J. Alloys Compd. **329**, 47 (2001).
[228] H. Noël, A. P. Gonçalves, Intermetallics, **9**, 473 (2001).
[229] P. Boulet, M. Vybornov, A. Simopoulos, A. Kostikas, H. Noël, P. Rogl, J. Alloys Compd. **283**, 49 (1999).

[230] V. H. Tran, R. Troć, F. Bourée, T. Roisnel, G. André, J. Magn. Magn. Mater. **140 – 144**, 1377 (1995).
[231] F. R. de Boer, E. Brück, H. Nakotte, A. V. Andreev, V. Sechovsky, L. Havela, P. Nozar, C. J. M. Denissen, K. H. J. Buschow, B. Vaziri, M. Meissner, H. Maletta, P. Rogl, Physica B **176**, 275 (1992).
[232] S. F. Matar, F. Mirambet, B. Chevalier, J. Etourneau, J. Magn. Magn. Mater. **140 – 144**, 1389 (1995).
[233] P. M. Oppeneer, A. N. Yaresko, A. Ya. Perlov, V. N. Antonov, H. Eschrig, Phys. Rev. B **54**, 3706 (1996).
[234] M. Yethiraj, R. A. Robinson, J. J. Rhyne, J. A. Gotaas, K. H. J. Buschow, J. Magn. Magn. Mater. **79**, 355 (1989).
[235] D. Kaczorowski, N. Stüßer, Solid State Commun. **100**, 43 (1996).
[236] F. Mirambet, B. Chevalier, P. Gravereau, J. Etourneau, Solid State Commun. **82**, 25 (1992).
[237] D. Kaczorowski, Z. Zołnierek, C. Geibel, F. Steglich, J. Alloys Compd. **200**, 115 (1993).
[238] F. Mirambet, P. Gravereau, B. Chevalier, L. Trut, J. Etourneau, J. Alloys Compd. **191**, L1 (1993).
[239] M. Lukachuk, R. Pöttgen, Z. Kristallogr. **218**, 767 (2003).
[240] M. Diviš, M. Richter, H. Eschrig, J. Alloys Compd. **255**, 11 (1997).
[241] P. Manfrinetti, F. Canepa, A. Palenzona, M. L. Fornasini, E. Giannini, J. Alloys Compd. **247**, 109 (1997).
[242] G. Principi, T. Spataru, A. Maddalena, A. Palenzona, P. Manfrinetti, P. Blaha, K. Schwarz, V. Kuncser, G. Filoti, J. Alloys Compd. **317 – 318**, 567 (2001).
[243] O. Moze, P. Manfrinetti, F. Canepa, A. Palenzona, M. L. Fornasini, J. R. Rodriguez-Carvajal, Intermetallics **8**, 273 (2000).